Science Advances
AAAS

advances.sciencemag.org/cgi/content/full/6/27/eaaz5548/DC1

Supplementary Materials for

The predictable chaos of slow earthquakes

A. Gualandi*, J.-P. Avouac, S. Michel, D. Faranda

*Corresponding author. Email: adriano.geolandi@gmail.com

Published 1 July 2020, *Sci. Adv.* **6**, eaaz5548 (2020)
DOI: 10.1126/sciadv.aaz5548

This PDF file includes:

Figs. S1 to S45

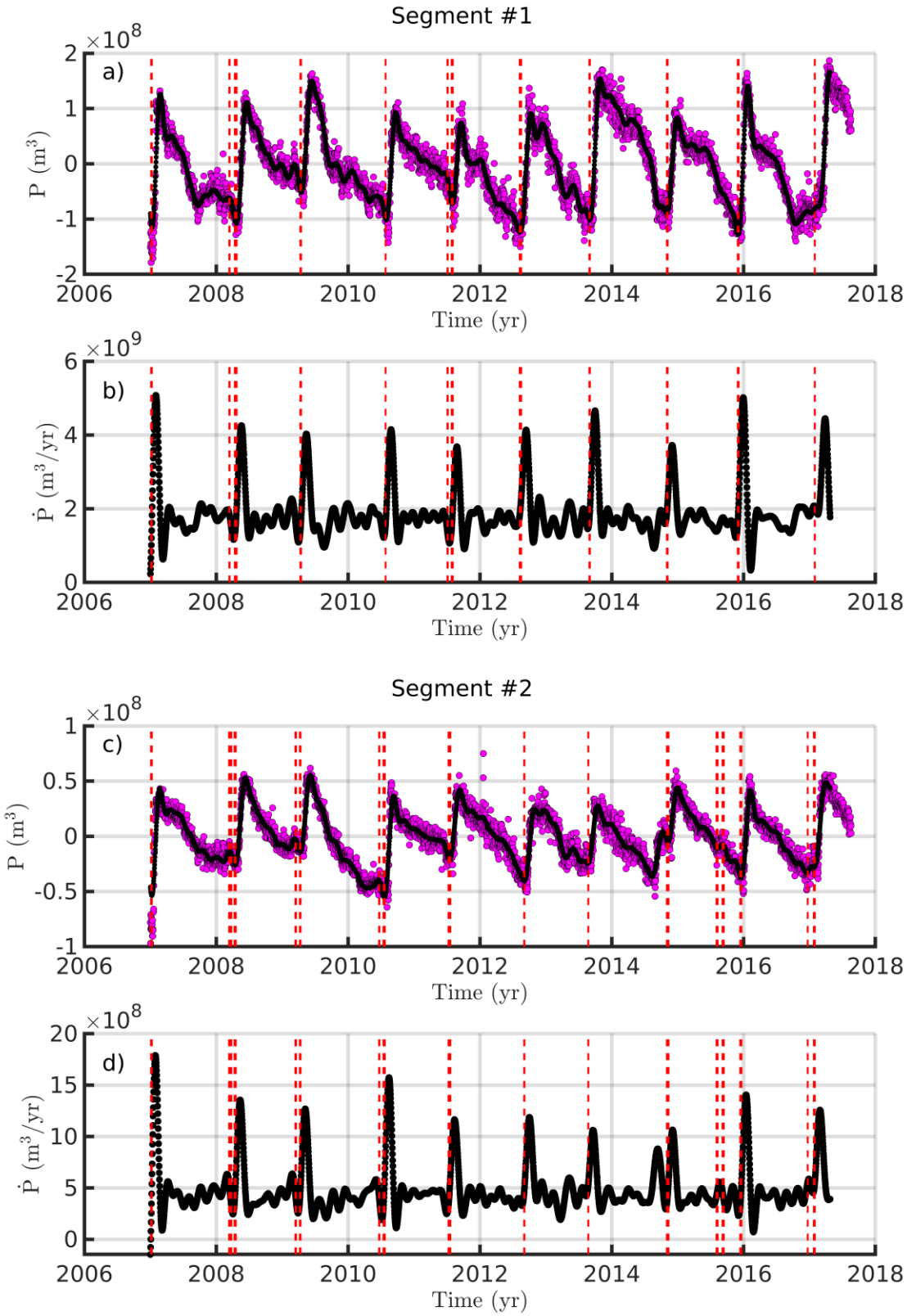

Fig. S1: As Fig. 2, but for segments #1 and #2. The red dashed lines are shown only for these two segments because they are the only ones exhibiting a significant low dimension (see Fig. 3).

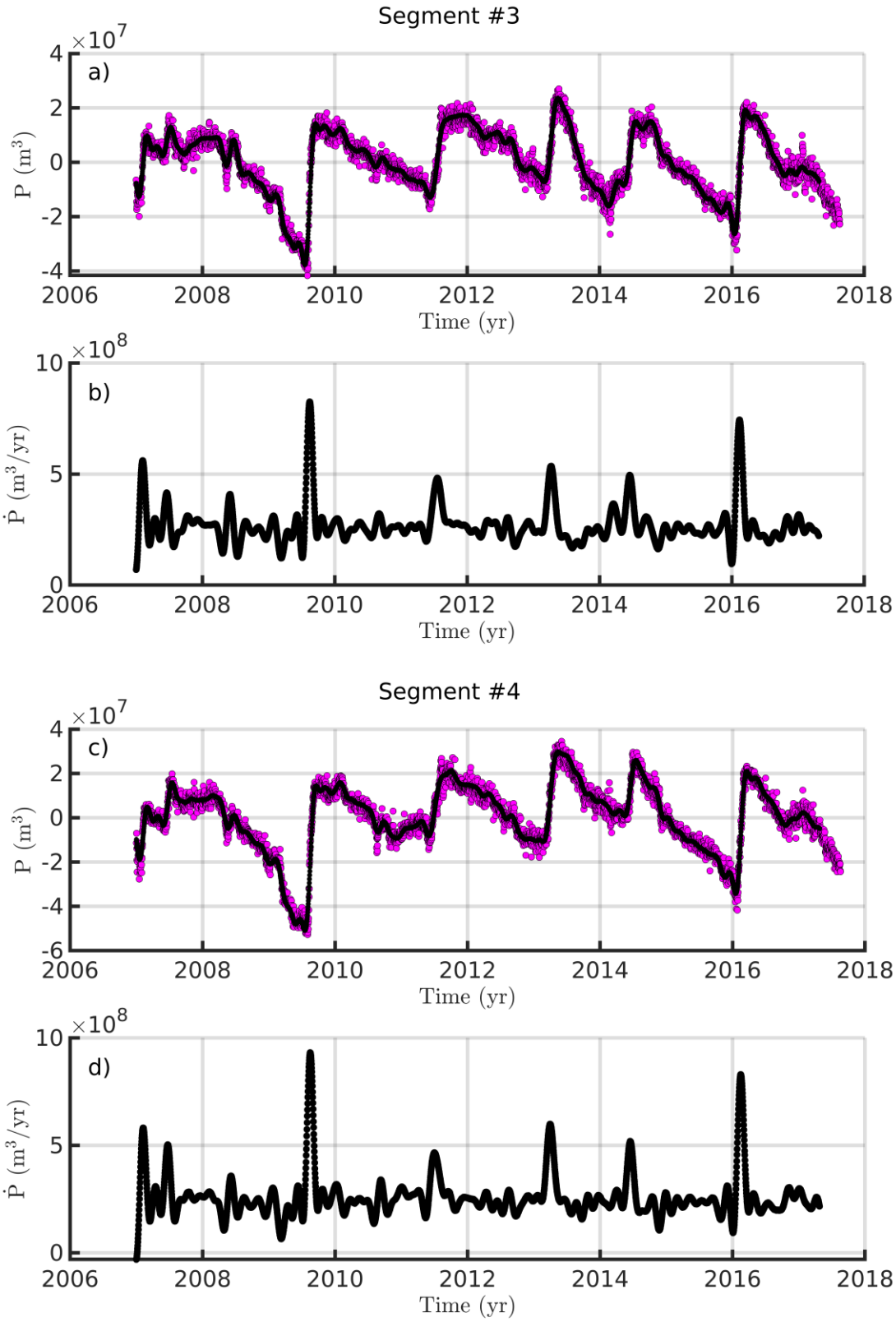

Fig. S2: As Fig. S1, but for segments #3 and #4.

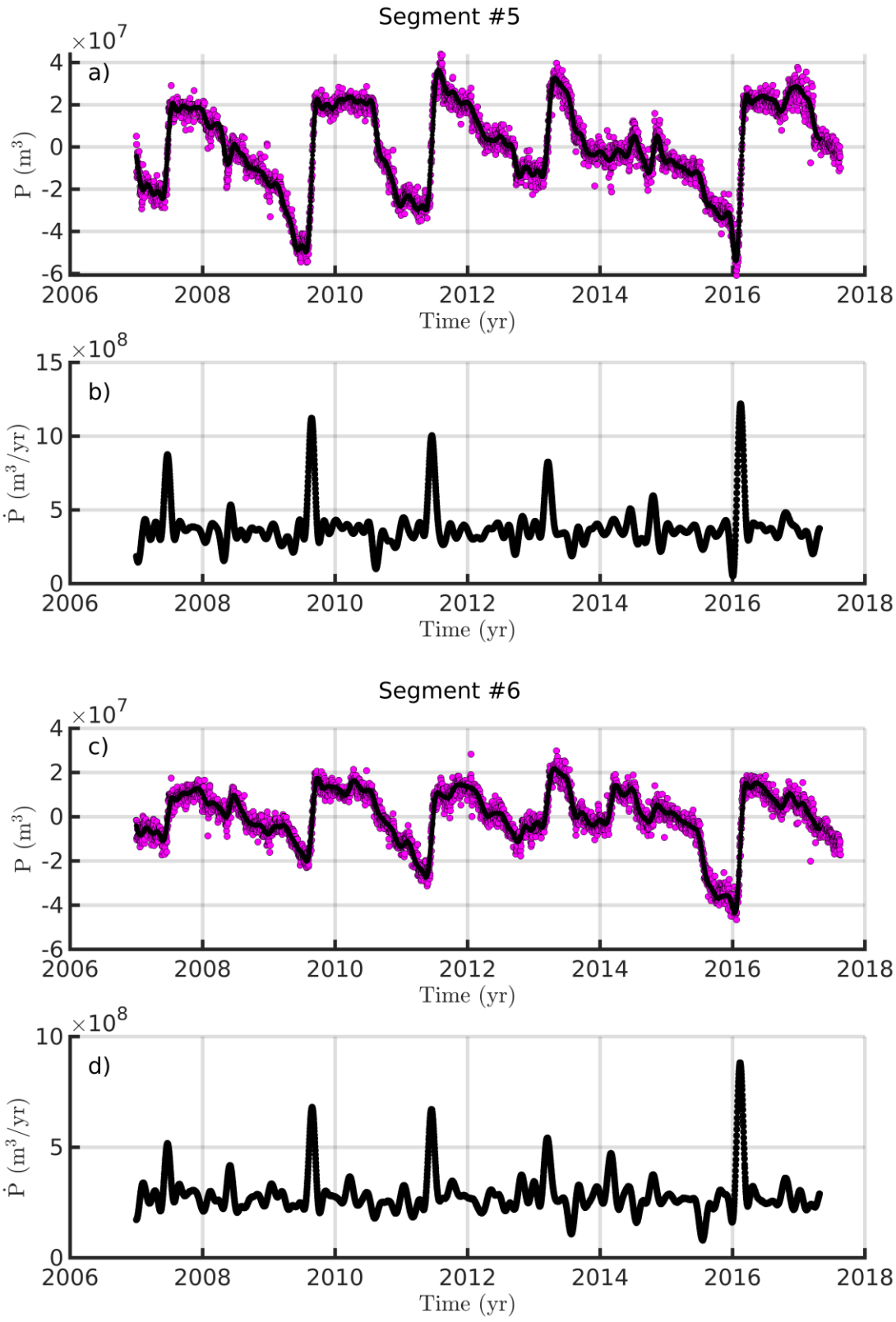

Fig. S3: As Fig. S1, but for segments #5 and #6.

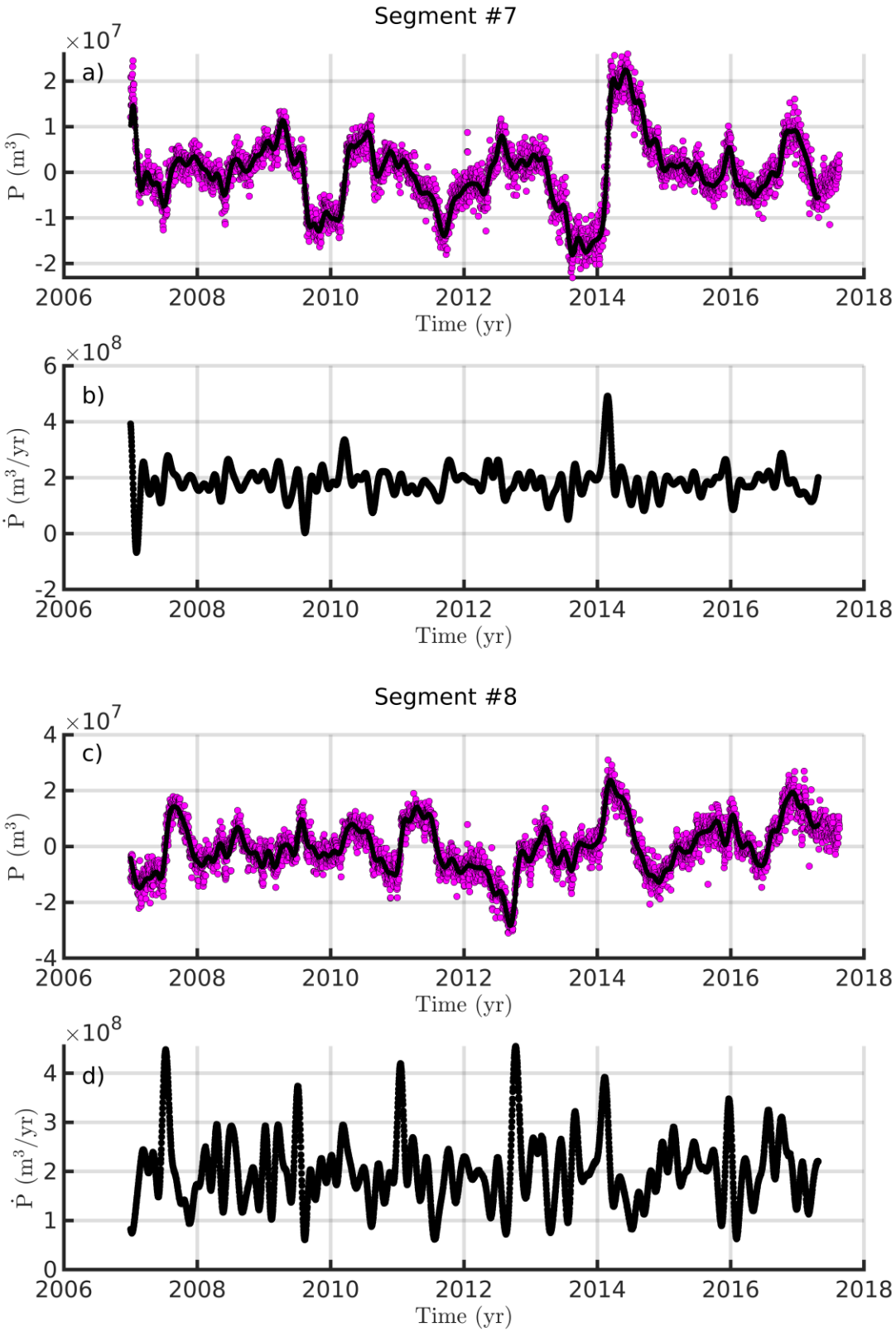

Fig. S4: As Fig. S1, but for segments #7 and #8.

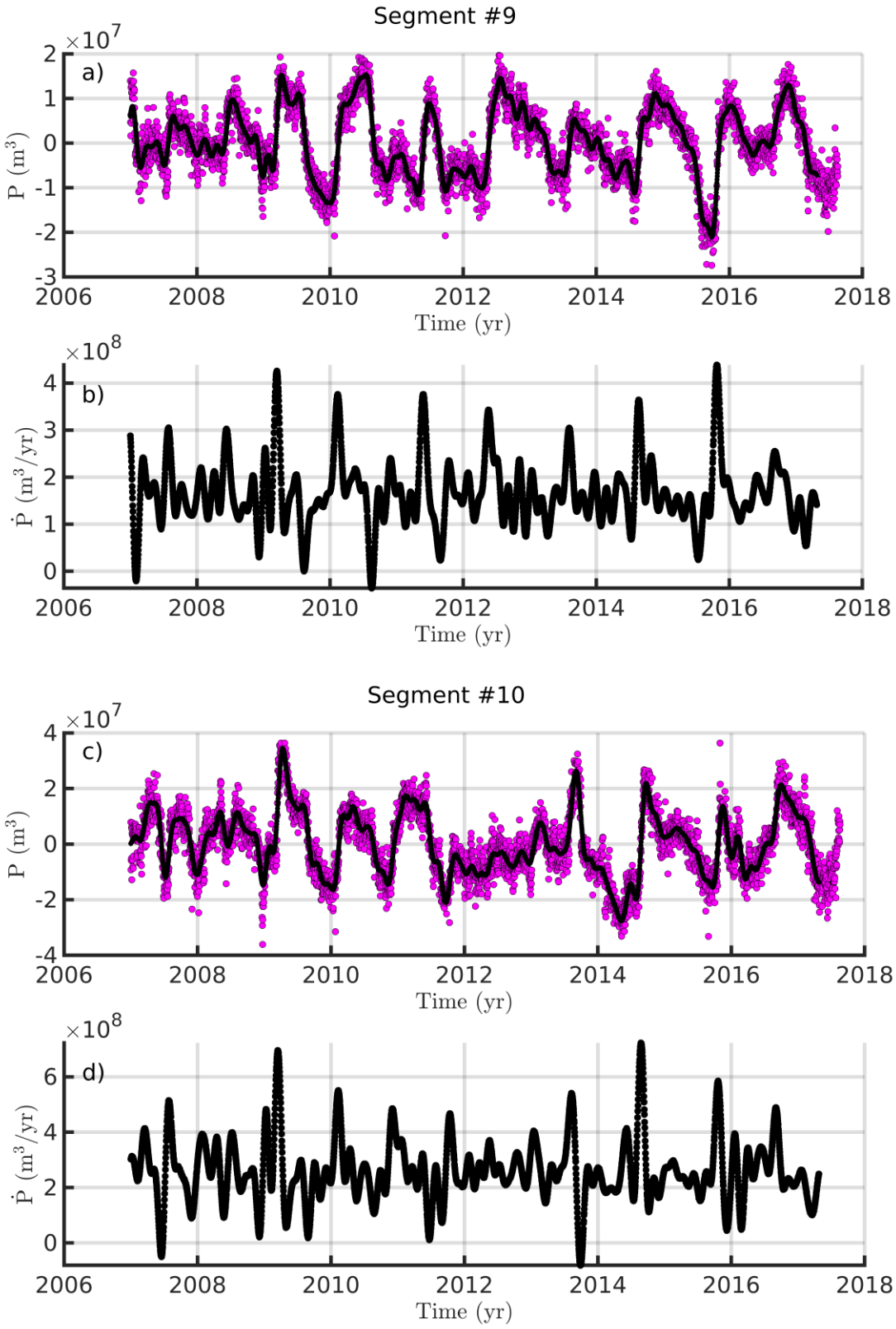

Fig. S5: As Fig. S1, but for segments #9 and #10.

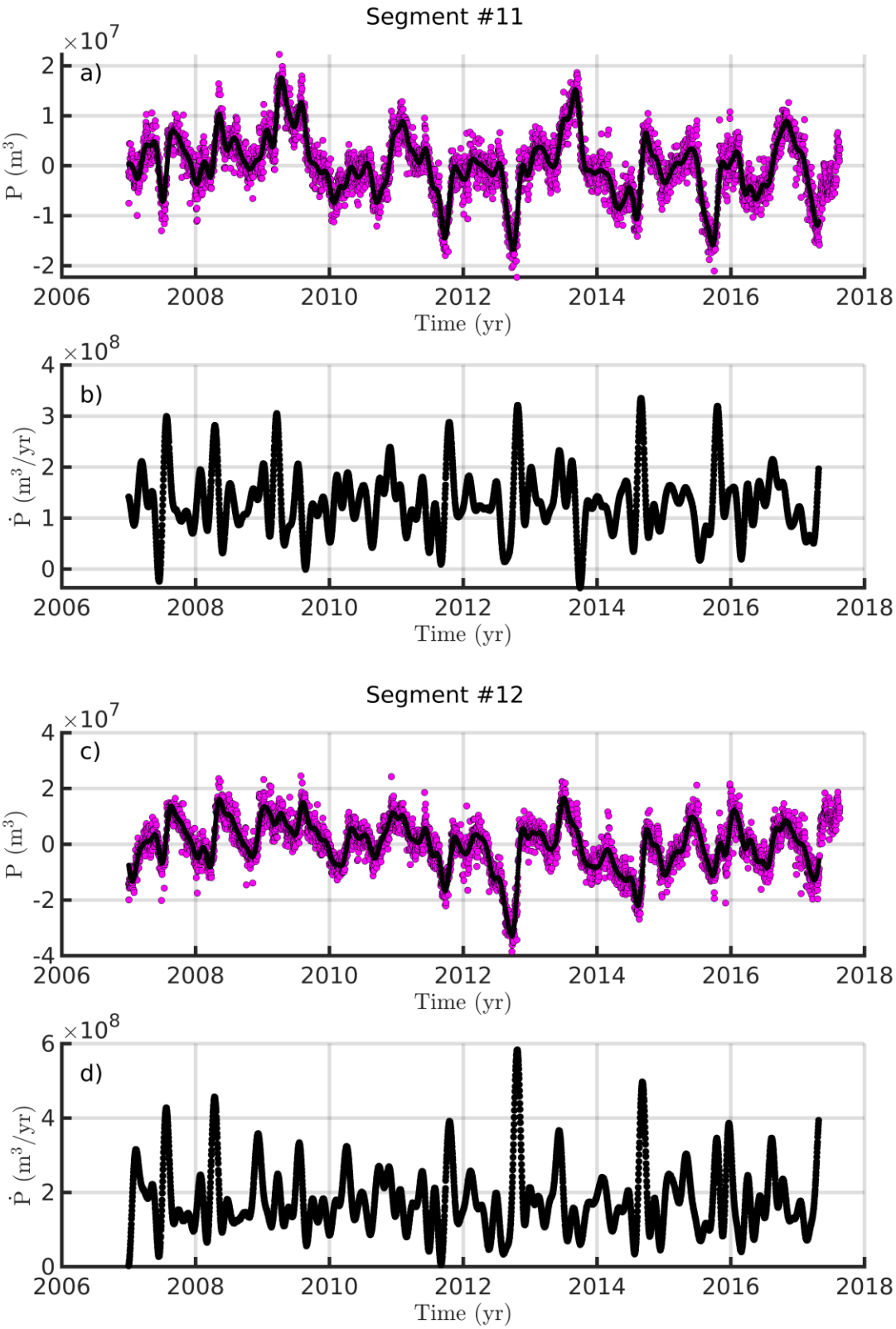

Fig. S6: As Fig. S1, but for segments #11 and #12.

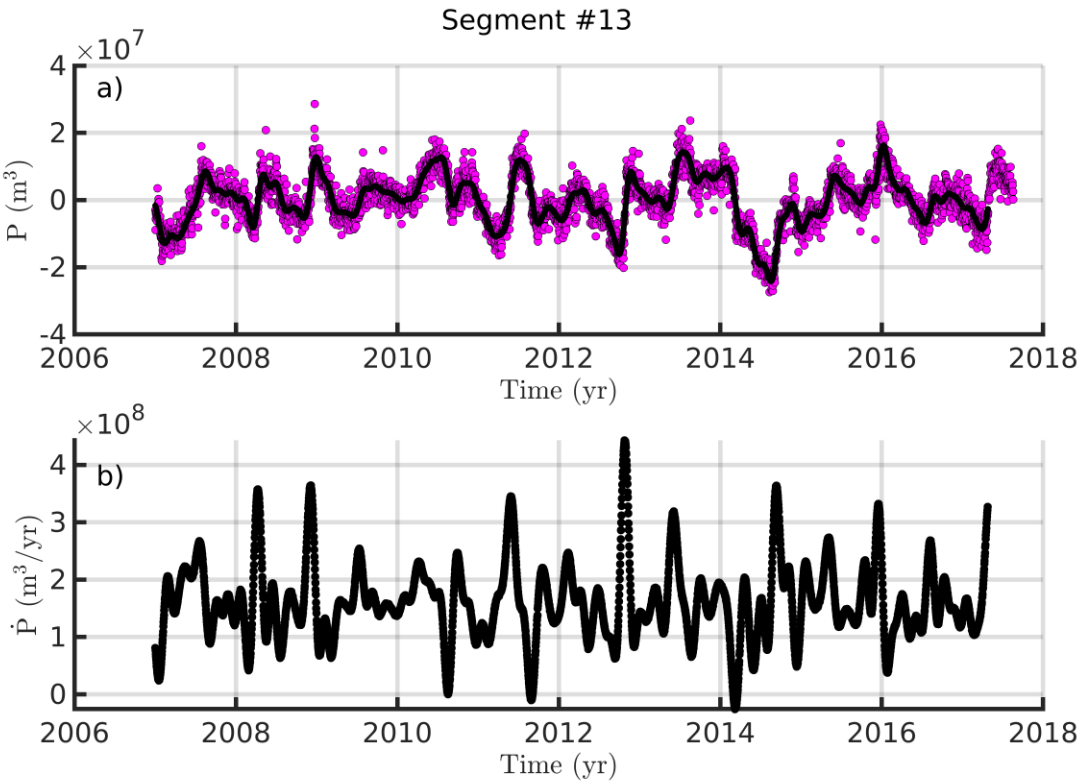

Fig. S7: As Fig. S1, but for segment #13.

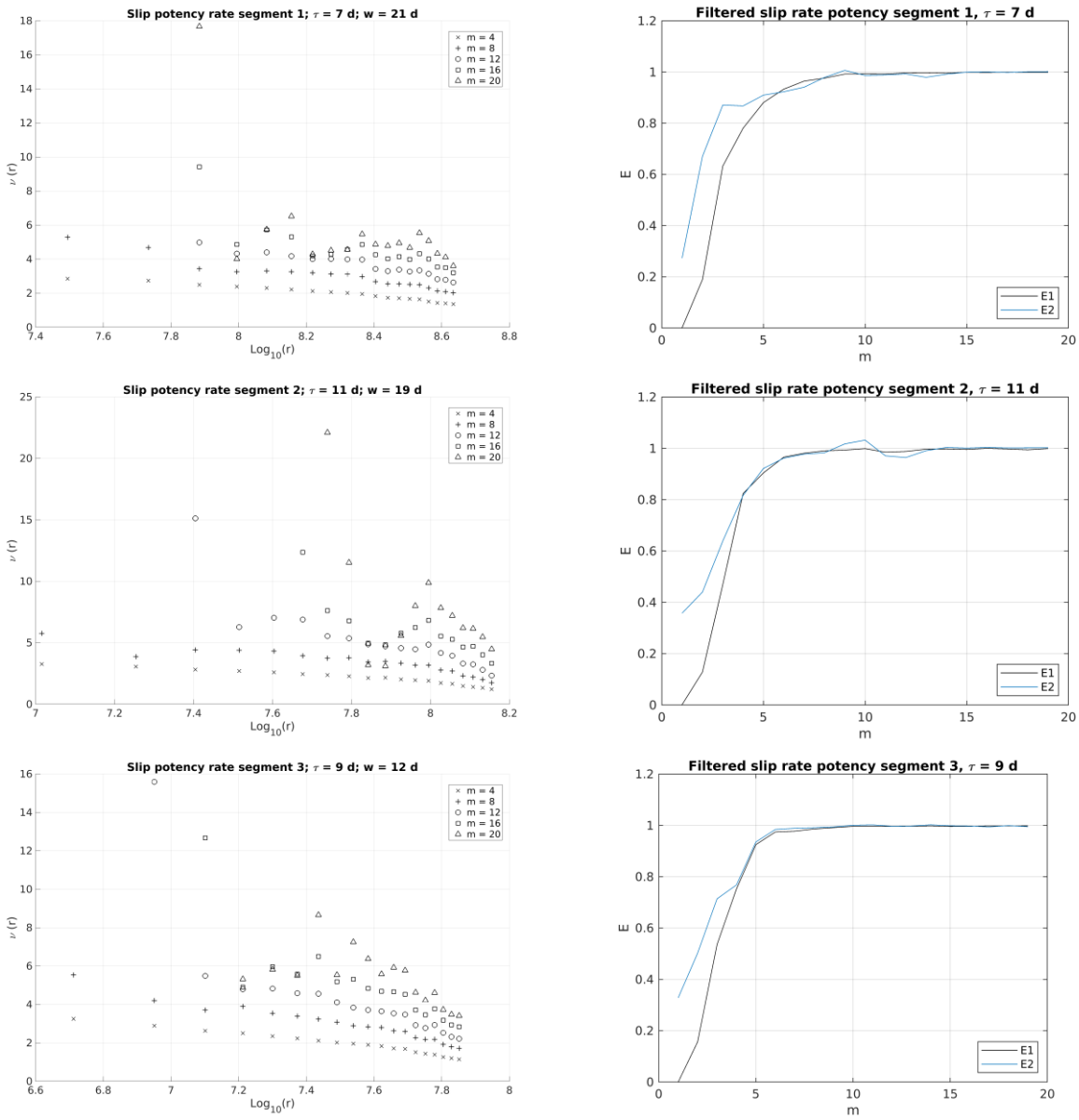

Fig. S8: ET results. Left: Correlation dimension ν vs Log(*r*) calculated on non-causally filtered slip potency rate time series (filter $EF_{1/35}^{1/21}$). Small value of *r* are dominated by noise, but a plateau becomes visible at around Log(*r*) 8.2, 7.8, and 7.2 for segments #1, #2, and #3, respectively. Right: False neighbors' metrics E_1 and E_2 calculated on causally filtered slip potency rate time series.

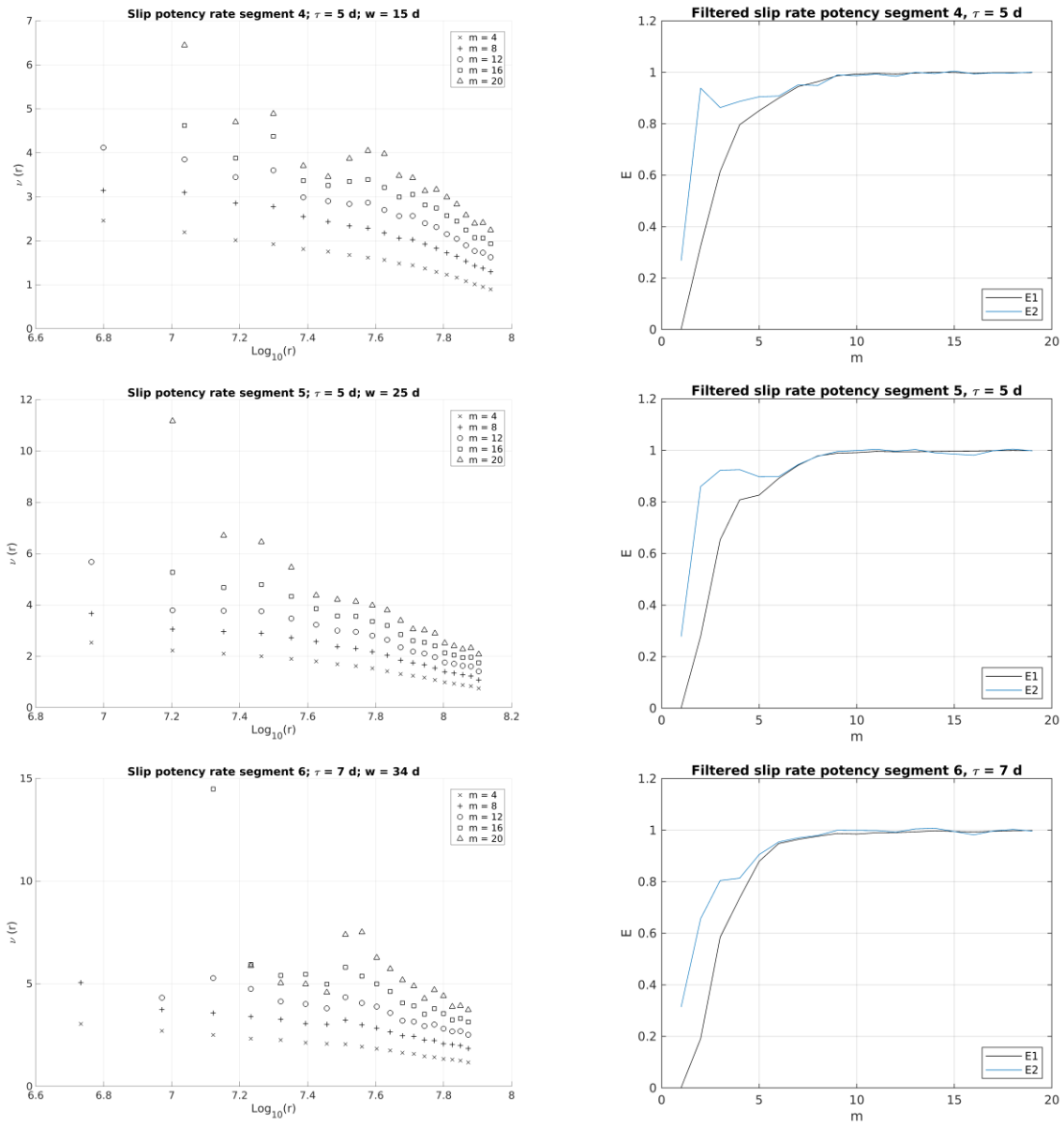

Fig. S9: Same as Fig. S8, but for segments #4, #5, and #6.

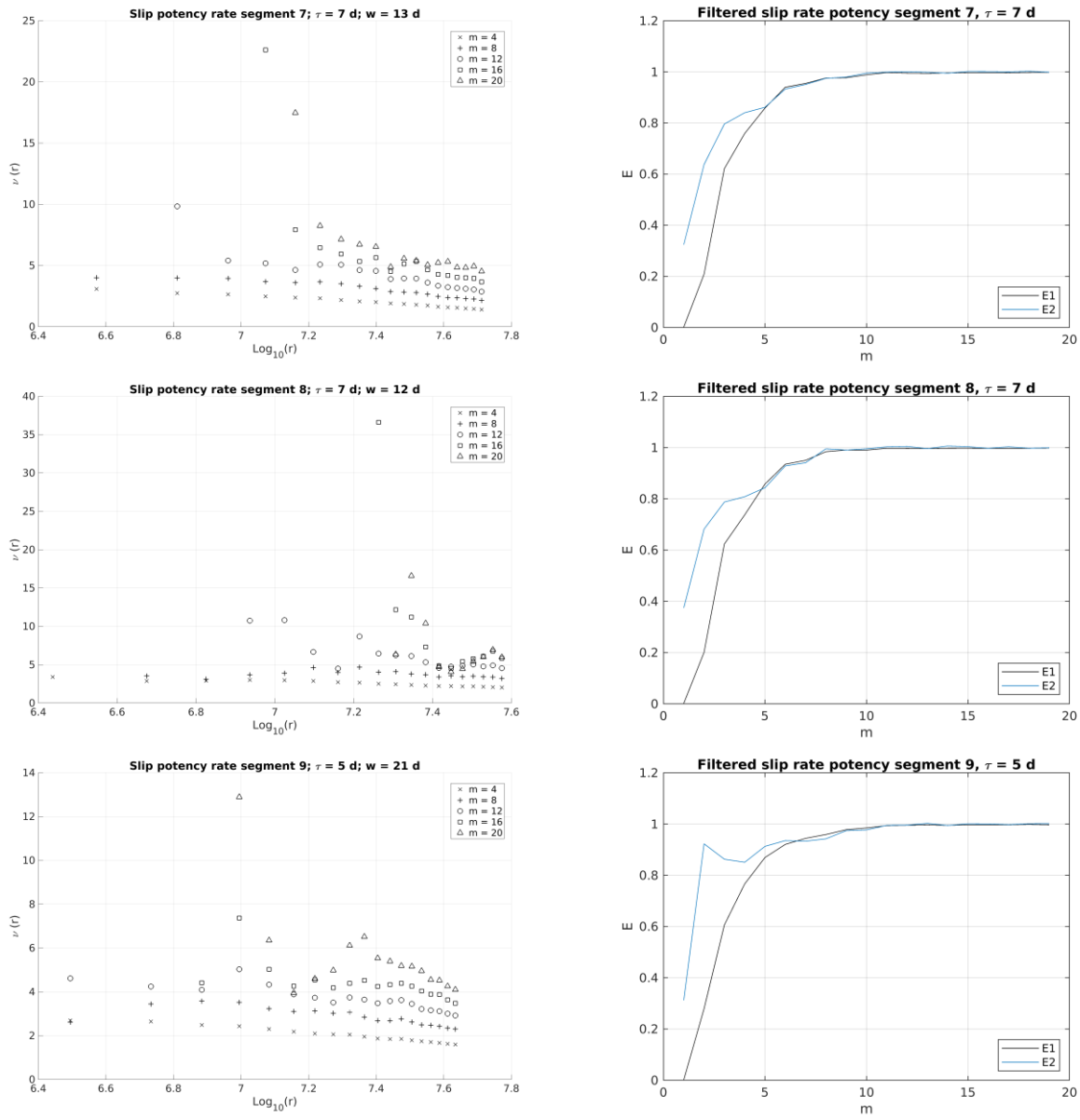

Fig. S10: Same as Fig. S8, but for segments #7, #8, and #9.

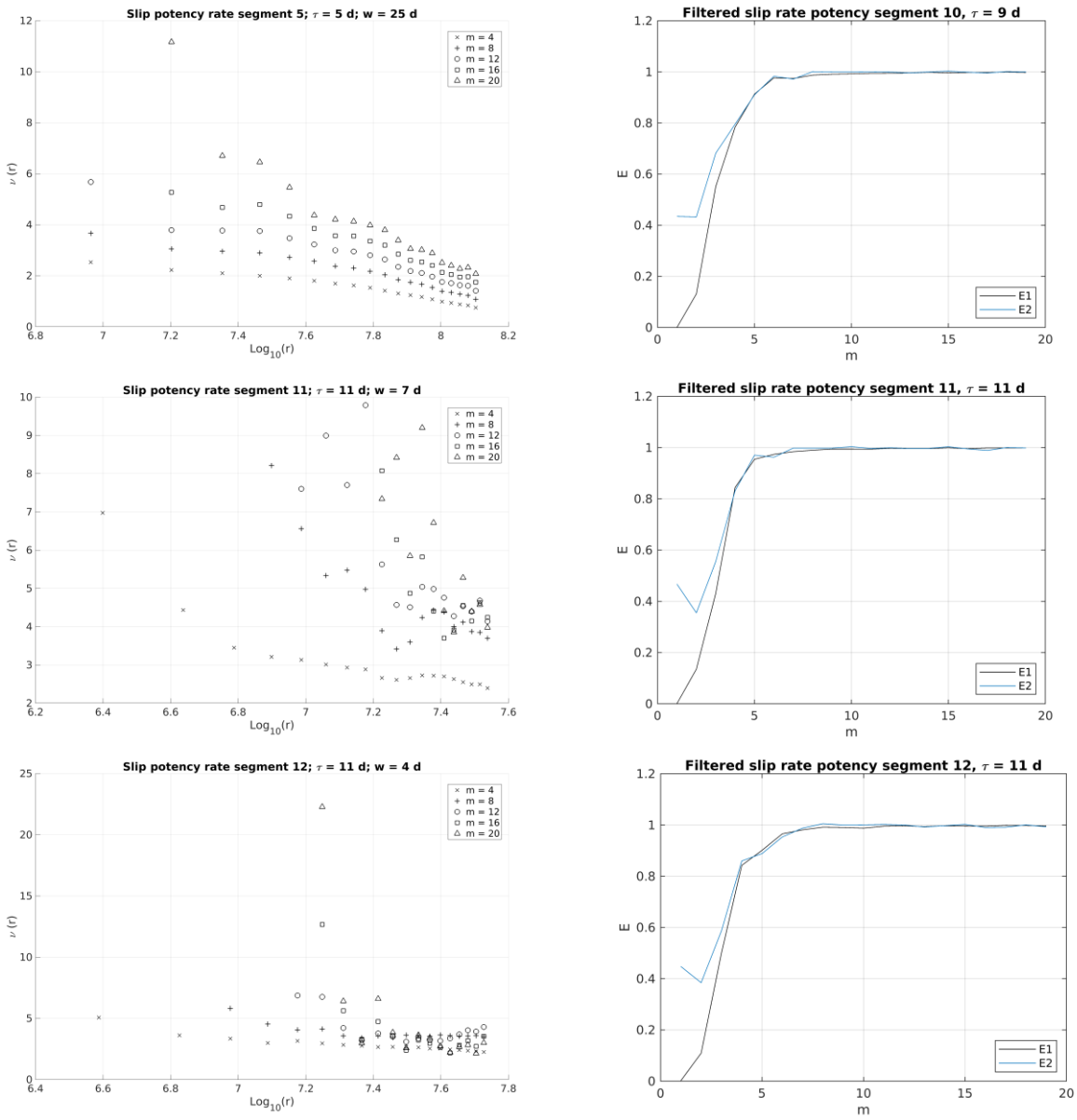

Fig. S11: Same as Fig. S8, but for segments #10, #11, and #12.

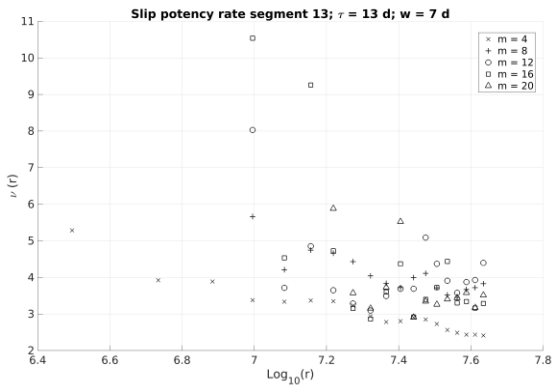

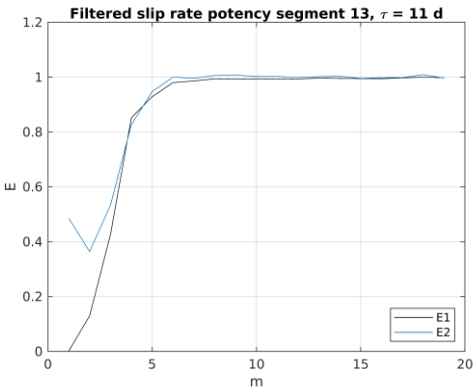

Fig. S12: Same as Fig. S8, but for segment #13.

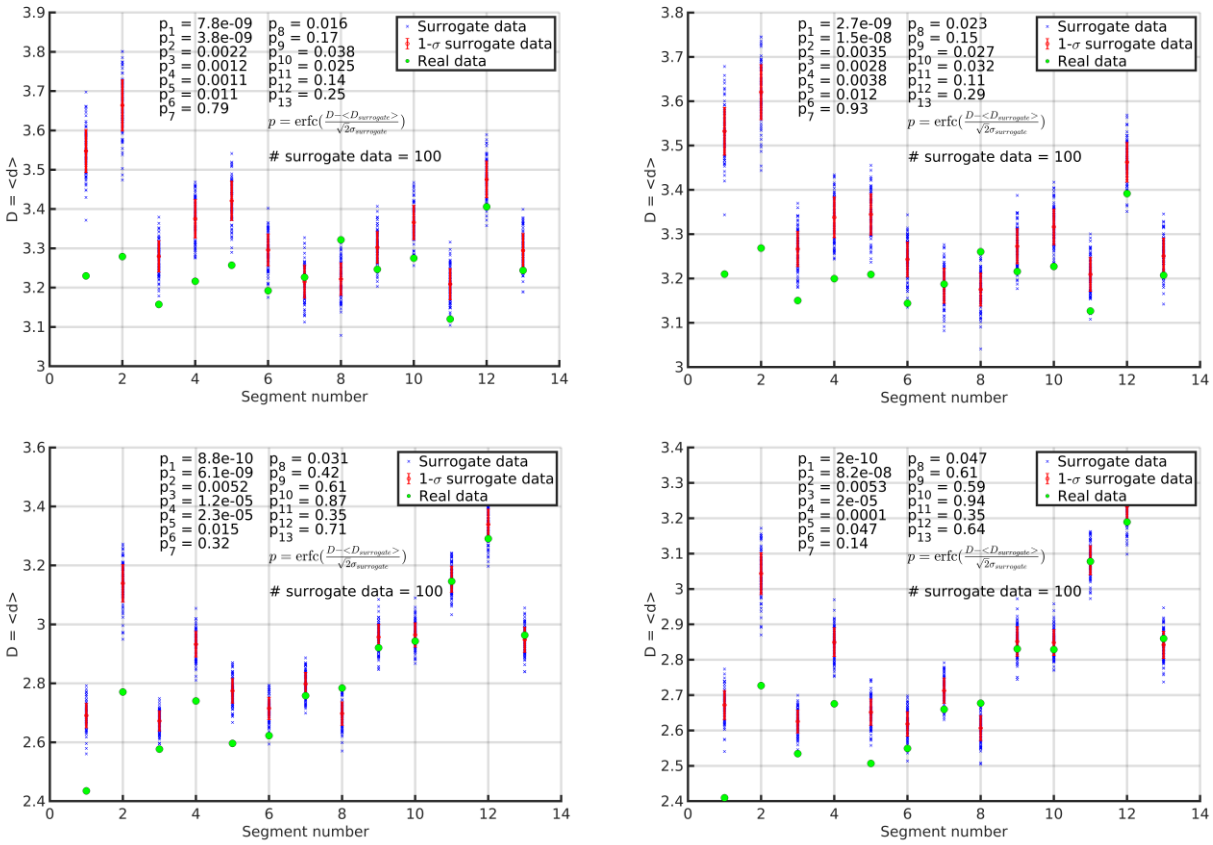

Fig. S13: Norm and quantile q effects for non-causally filtered time series (filter $EF_{1/35}^{1/21}$). Top-left: L1 norm, q = 0.98; top-right: L2 norm, q = 0.98; bottom-left: L1 norm, q = 0.99; bottom-right: L2 norm, q = 0.99.

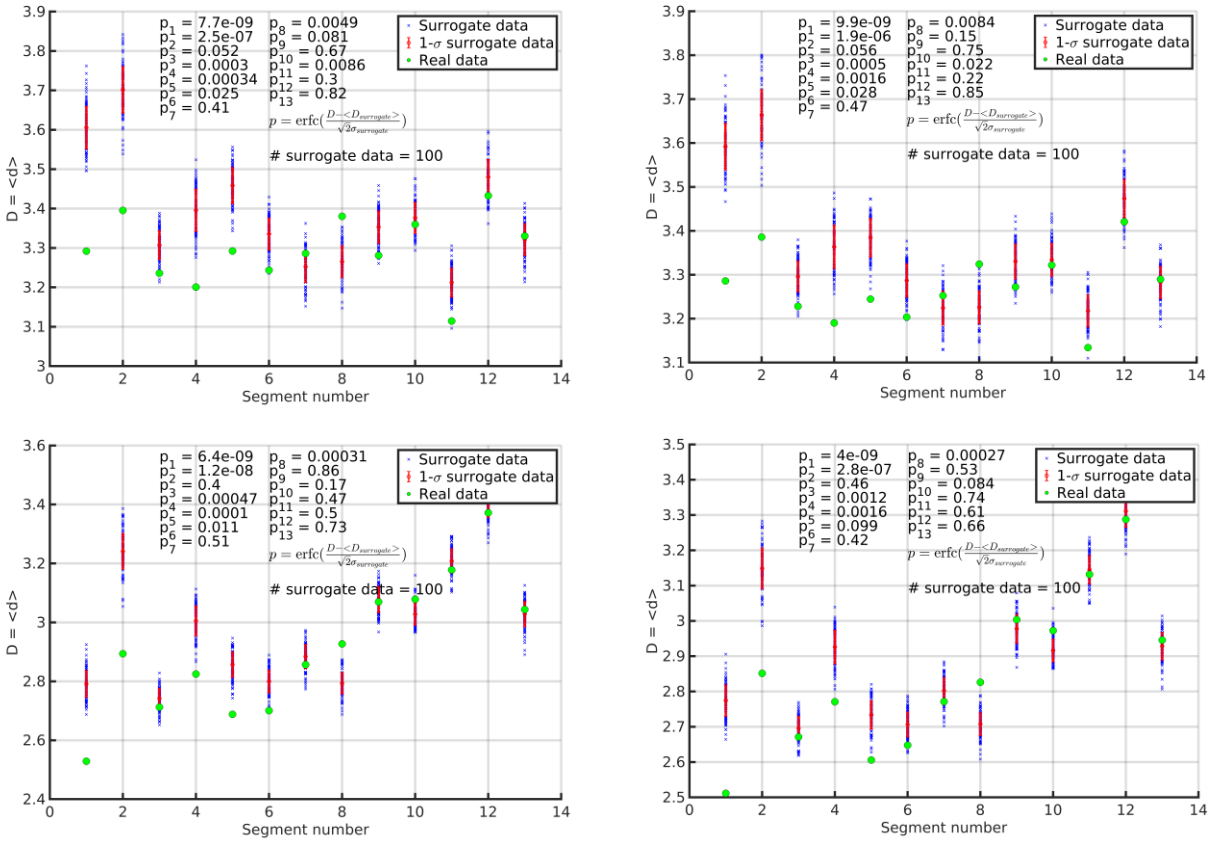

Fig. S14: Same as Fig. S13, but for causally filtered time series.

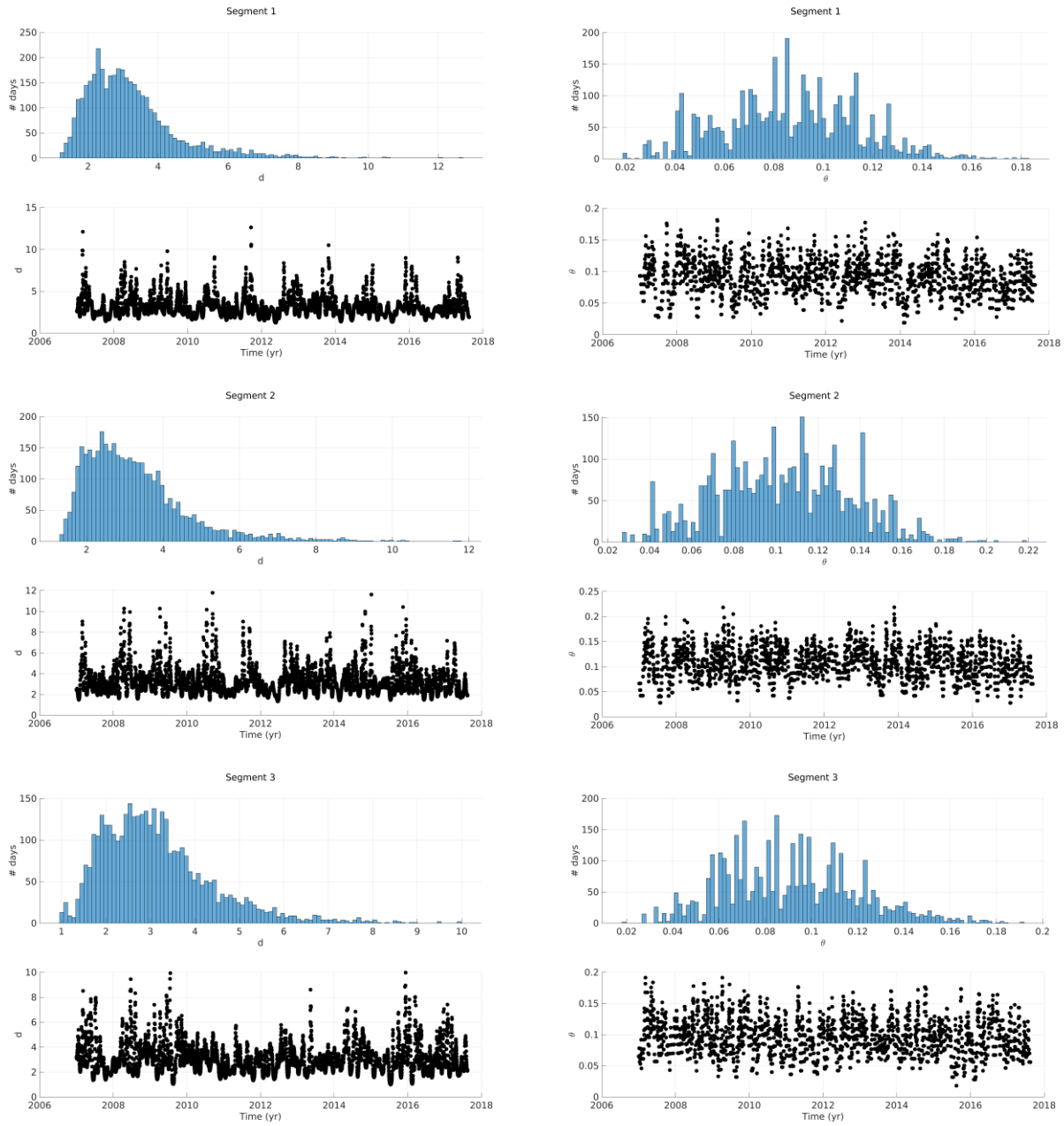

Fig. S15: Instantaneous dimension d and instantaneous extremal index θ. The statistics are shown for non-causally filtered (filter $\mathrm{EF}_{1/35}^{1/21}$) time series for segments #1, #2, and #3. For each statistics, the top panel is the histogram of the instantaneous values, and the bottom panel shows the temporal evolution.

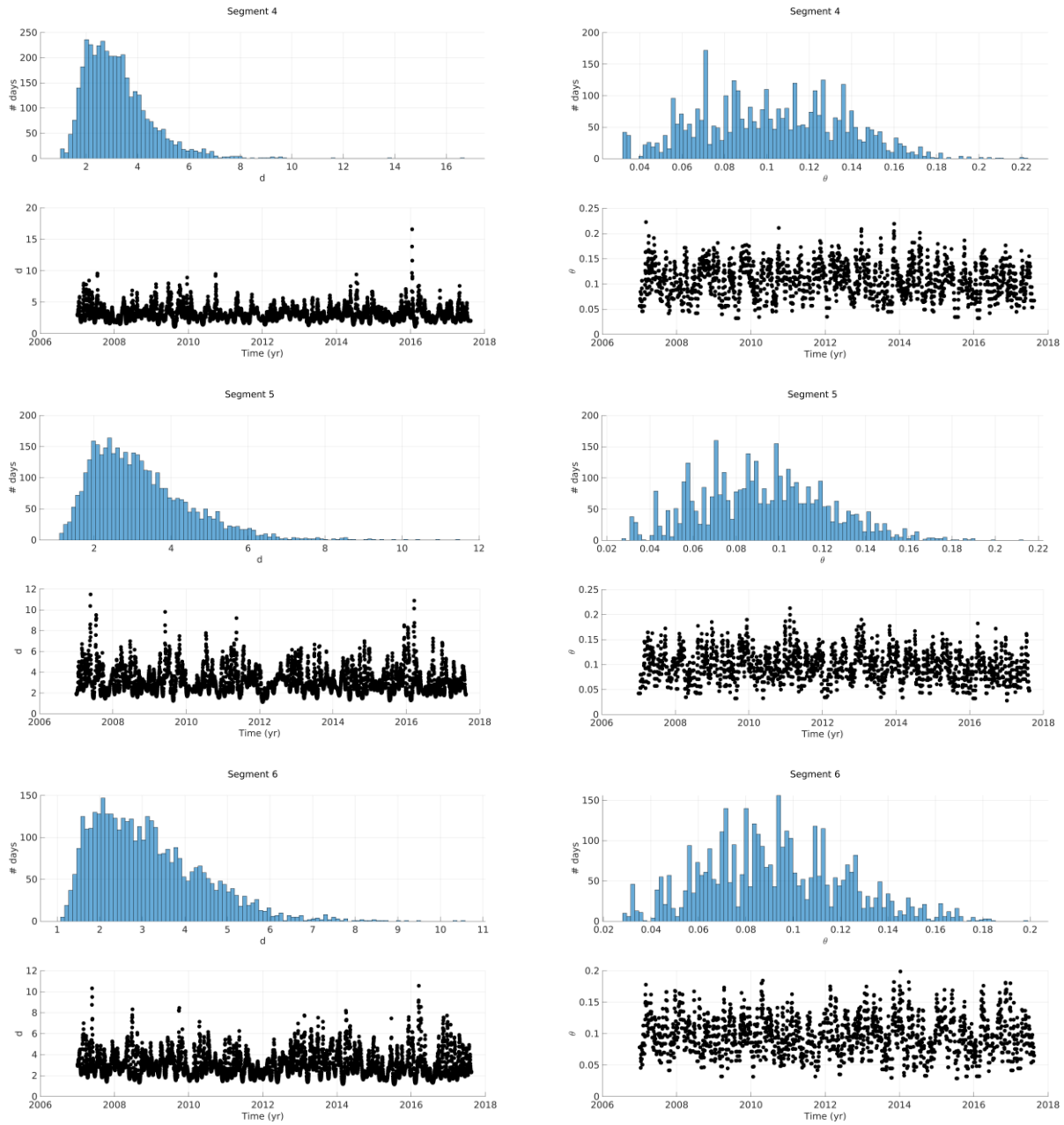

Fig. S16: Same as Fig. S15, but for segments #4, #5, and #6.

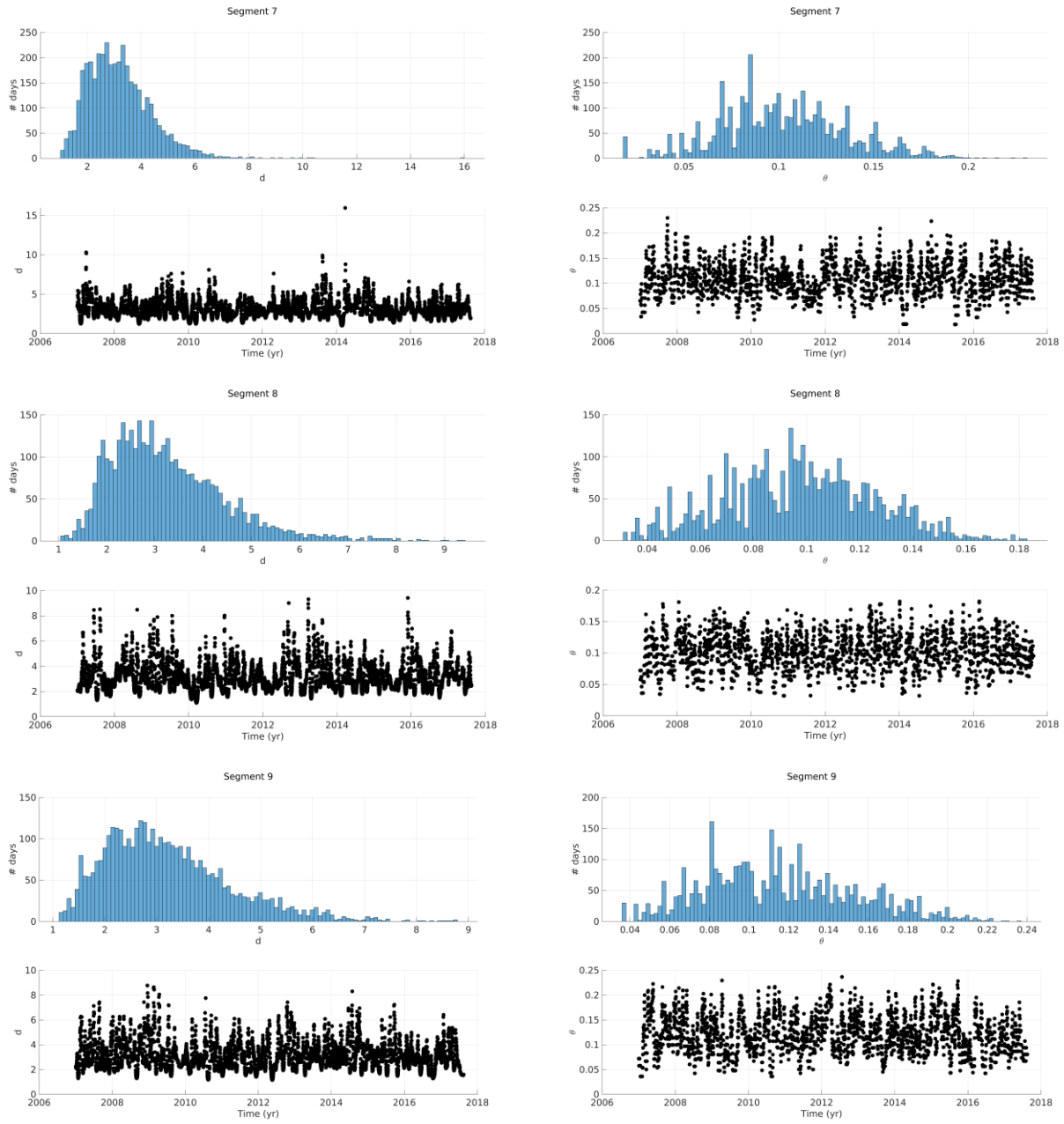

Fig. S17: Same as Fig. S15, but for segments #7, #8, and #9.

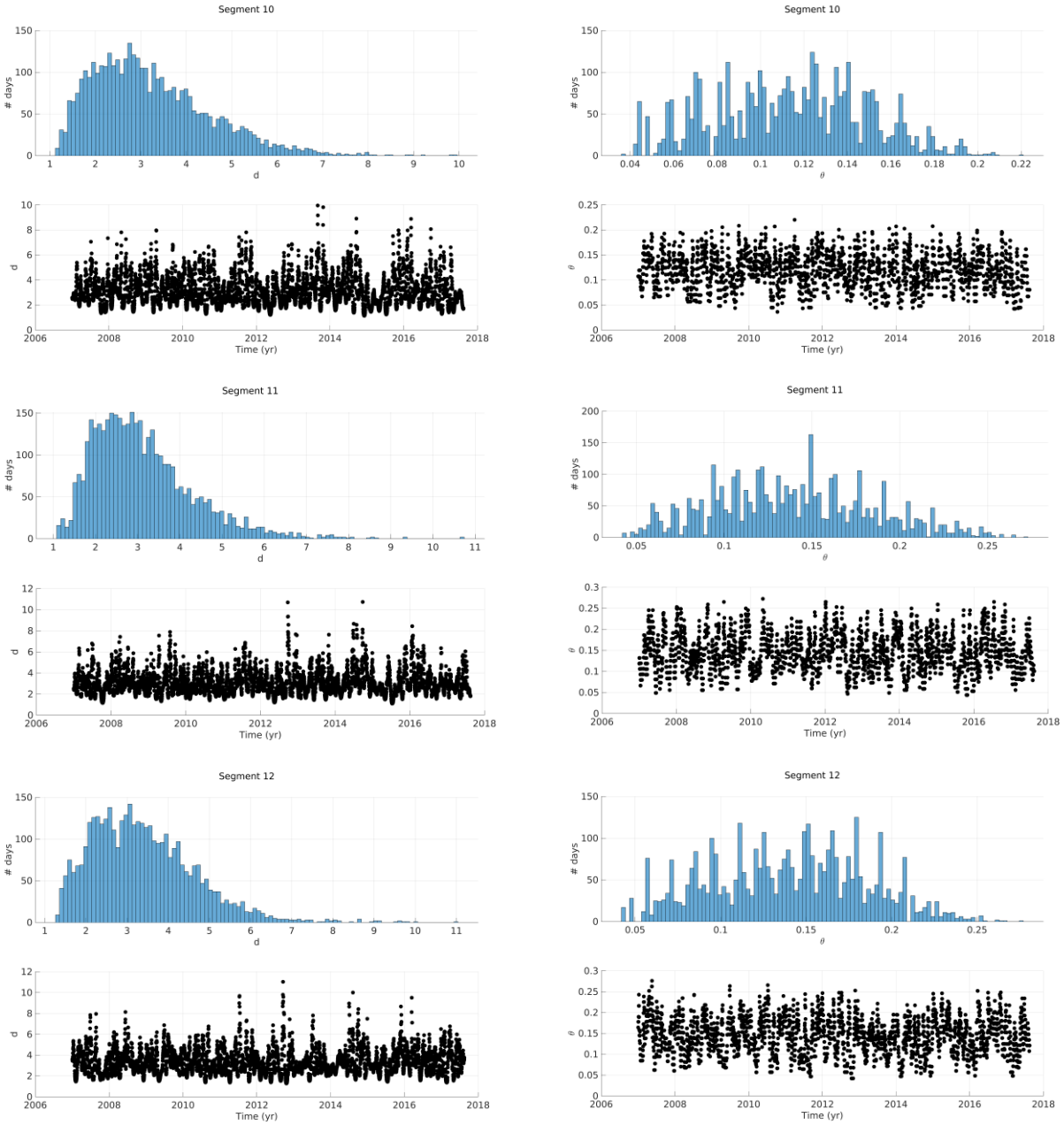

Fig. S18: Same as Fig. S15, but for segments #10, #11, and #12.

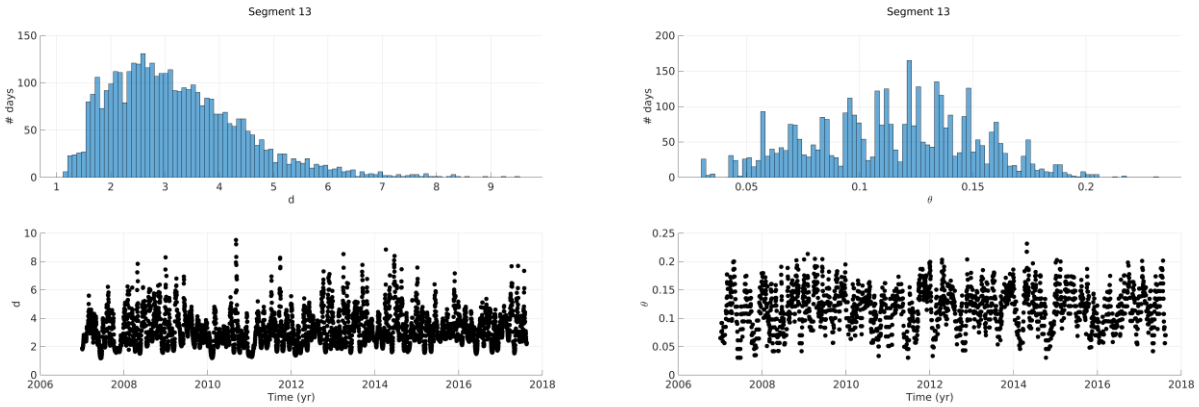

Fig. S19: Same as Fig. S15, but for segment #13.

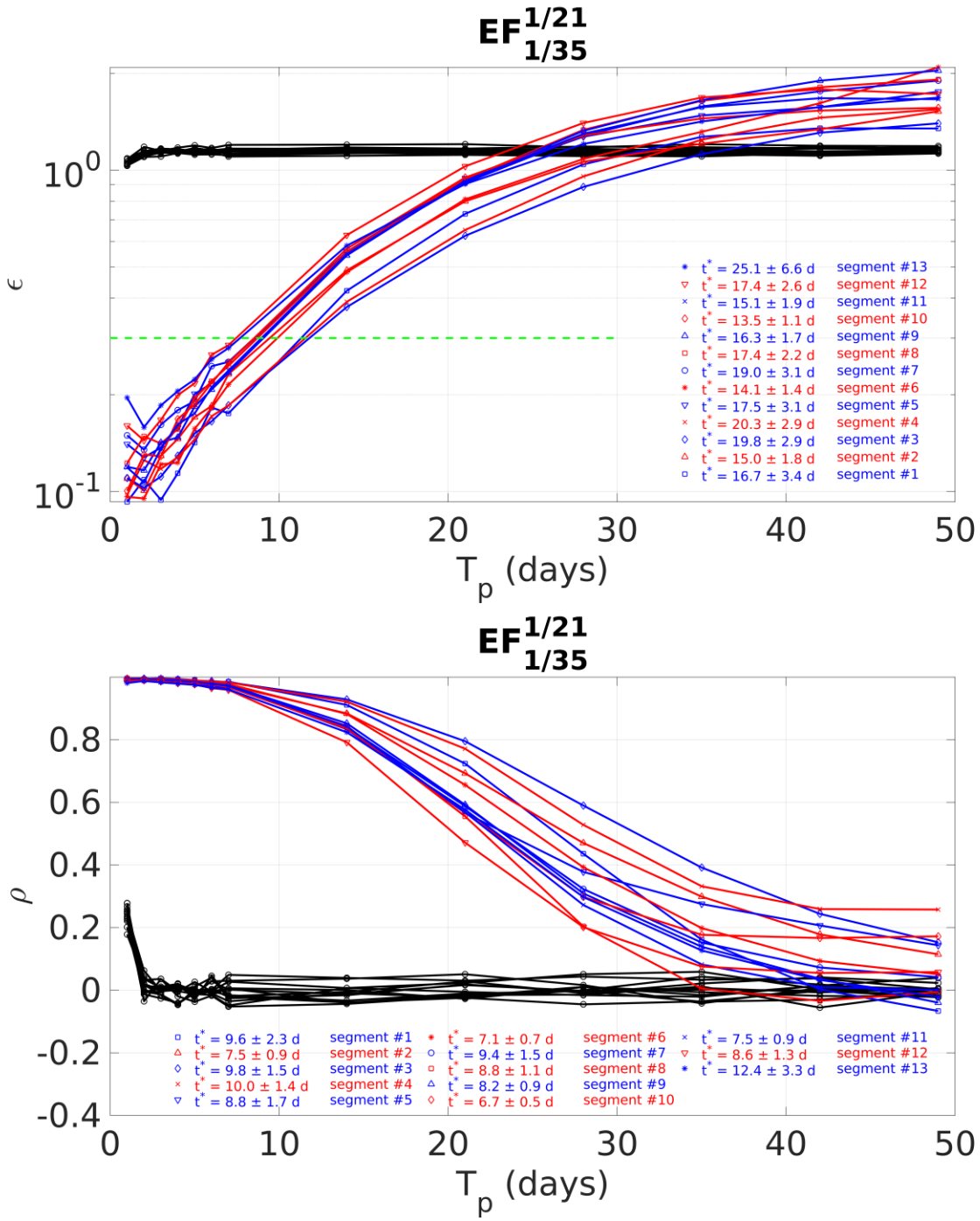

Fig. S20: NFA results on all segments time series unfiltered (black lines) and filtered using the $\mathrm{EF}_{1/35}^{1/21}$ filter (red and blue lines). These plots refer to embeddings with $\tau = 7$ days and $m = 9$. Top panel: Normalized prediction error ϵ as a function of the prediction time T_p. Equation (S14) to estimate H is valid for $\epsilon \ll 1$, and $t^* = 1/H$ values are calculated using points below the green dashed line $\epsilon^* = 0.3$. Bottom panel: Correlation ρ as a function of prediction time T_p. We use the points for which $\rho \geq 0.98$ to estimate H from equation (S15). Both statistics (ϵ and ρ) are almost constant for unfiltered time series and degrade when increasing the prediction time for filtered time series. This indicates that the high-frequency noise dominates in unfiltered time

series, resulting in statistics characteristic of a stochastic system, while the filtering step let the dynamics of the system emerge clearly.

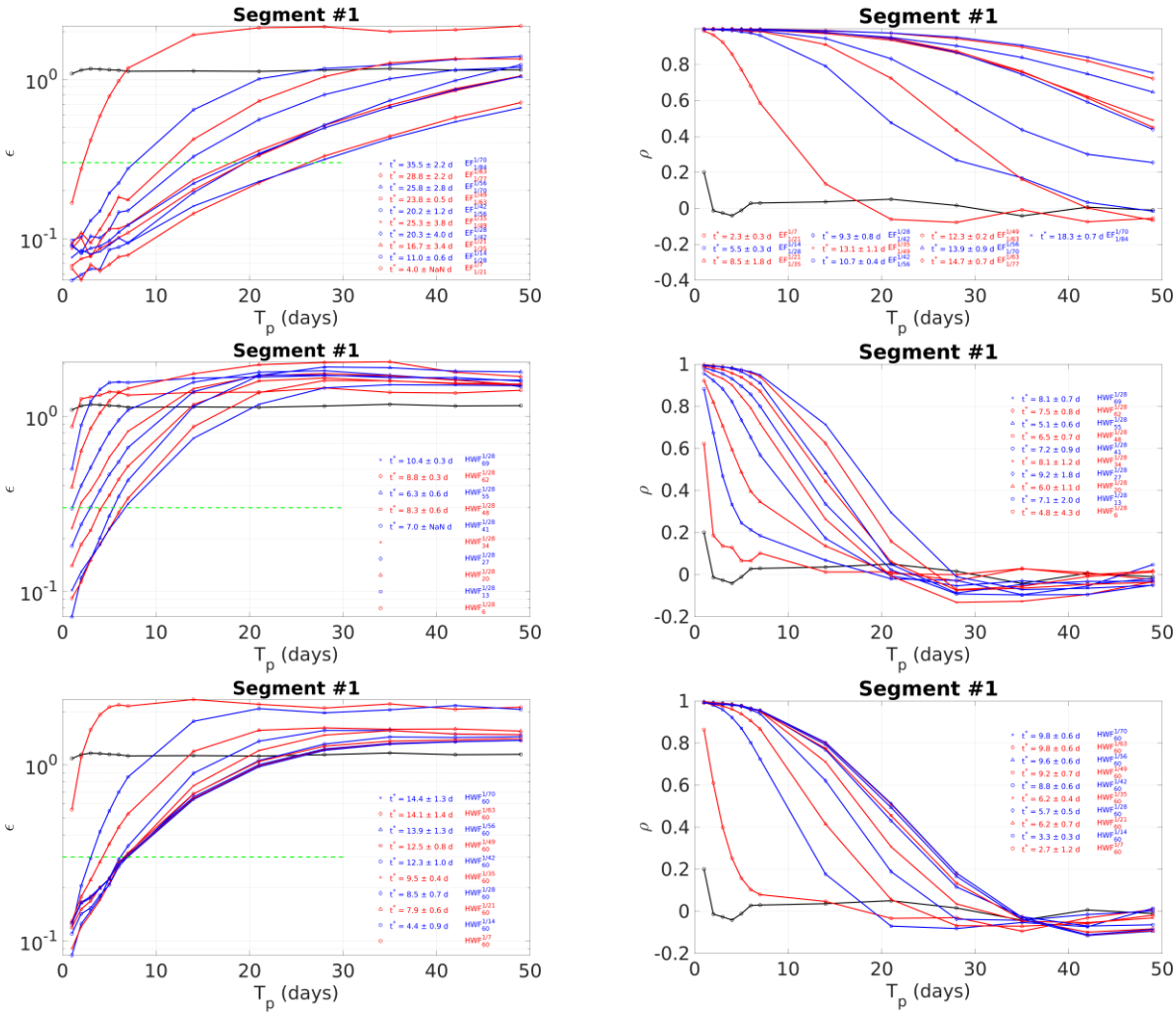

Fig. S21: Same as Fig. S20 but for only segment #1 and different filters. Left column: Normalized prediction error ϵ as a function of the prediction time T_p. Right column: Correlation ρ as a function of prediction time T_p. The estimate of H from the right column plots is now performed using the first 3 data points for all the tested filters. Top, central and bottom rows refer to the EF, HWF with constant $f_{cutoff} = 1/28$ and HWF with constant $N_b = 60$, respectively.

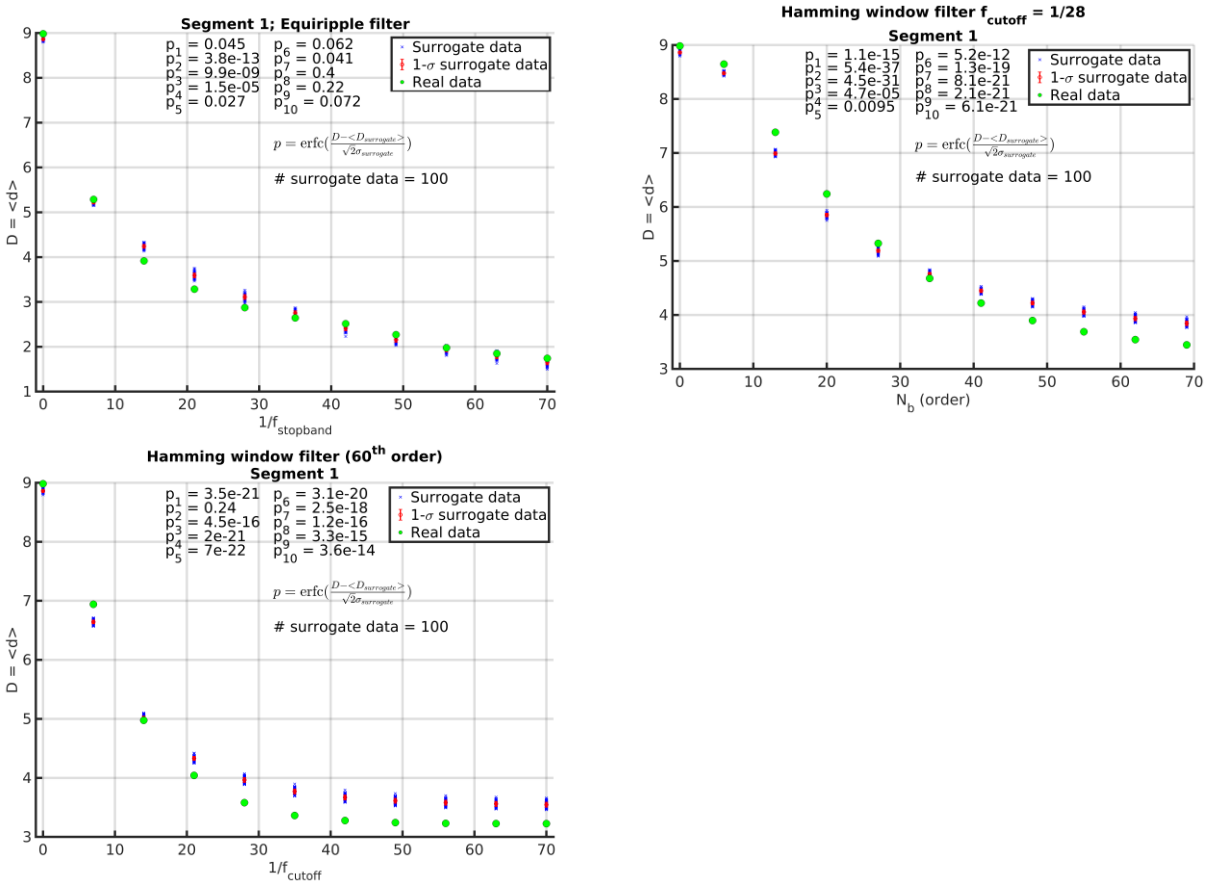

Fig. S22: Surrogate data test on the estimate of D via EVT (using an L2 norm and a quantile q = 0.98) for segment #1 for different filters and filter parameters. The point with abscissa 0 corresponds to the case of unfiltered data: the value estimated from the data (green dot) is not distinguishable from the surrogate data estimates, and we cannot reject the null hypothesis for which the data were generated by a linear stochastic model. The reported p-values indicate the degree of confidence at which the null hypothesis can be rejected for various filter paramters. They are sorted from left to right, i.e. with increasing abscissa.

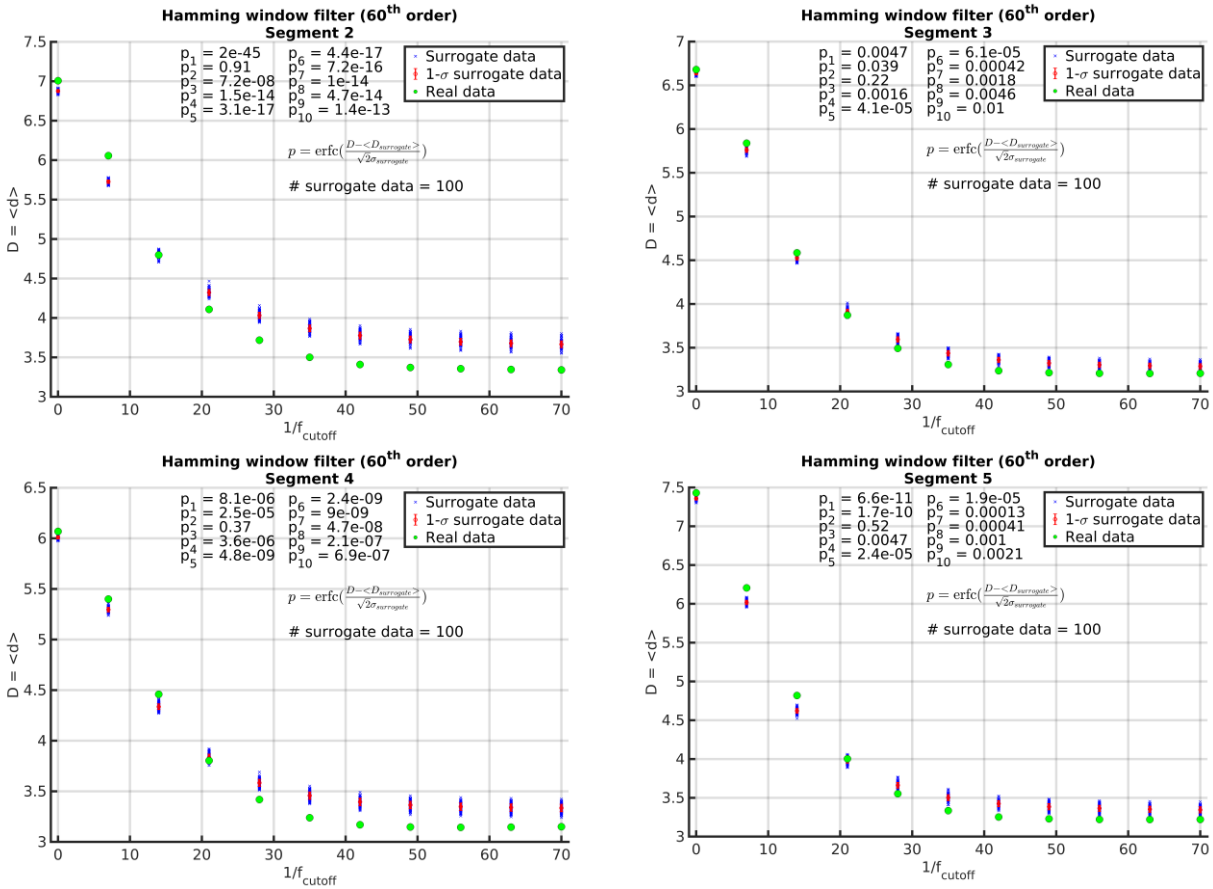

Fig. S23: Surrogate data test as in Fig. S22 using a Hamming window filter of the 60th order, but for segments #2, #3, #4, and #5.

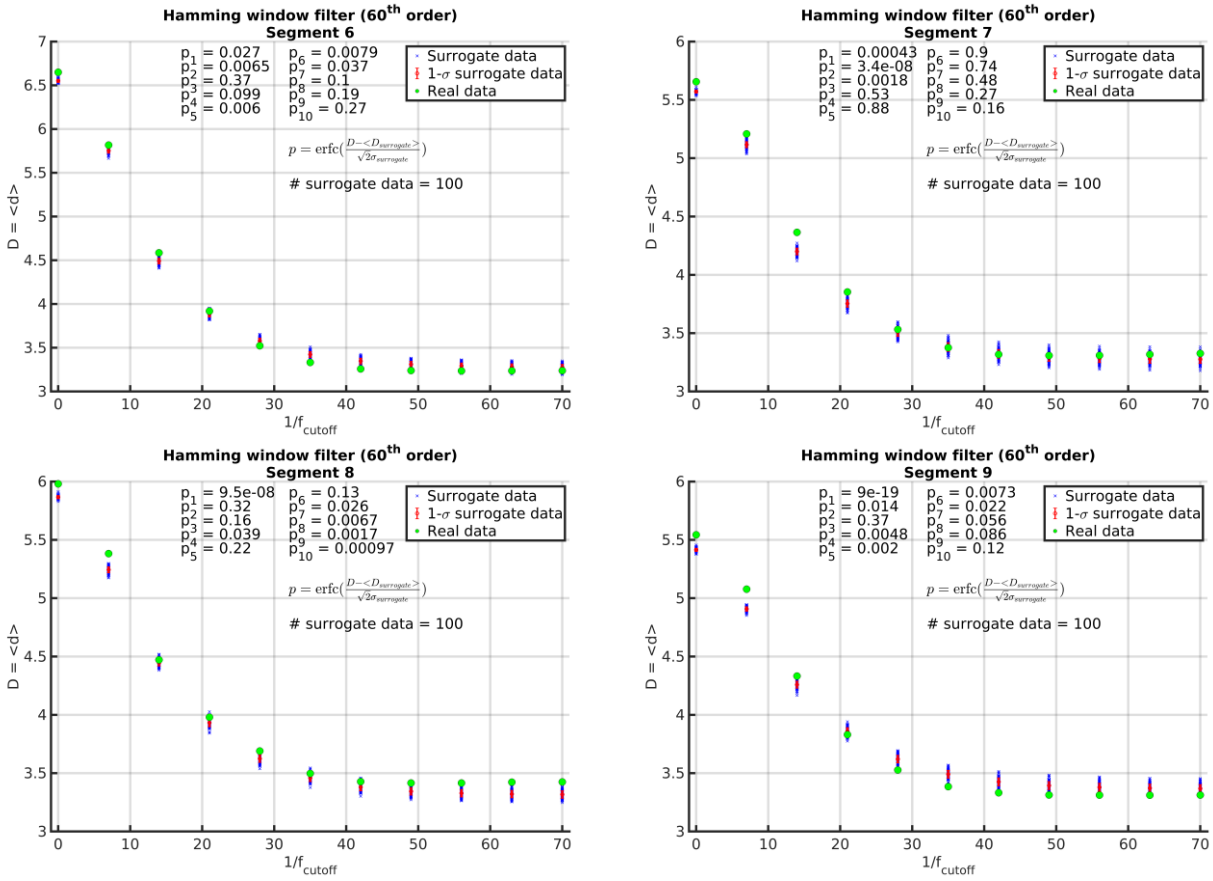

Fig. S24: Same as Fig. S23, but for segments #6, #7, #8, and #9.

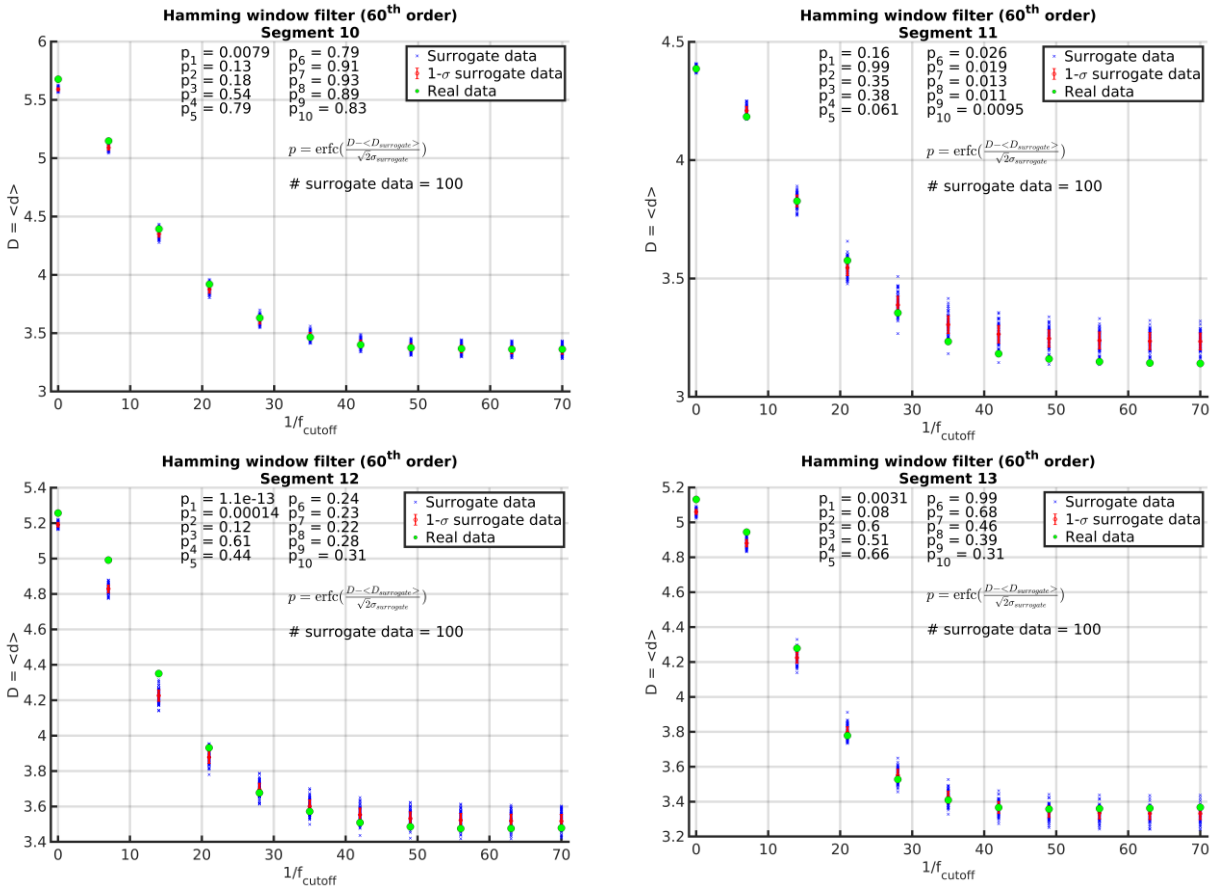

Fig. S25: Same as Fig. S23, but for segments #10, #11, #12, and #13.

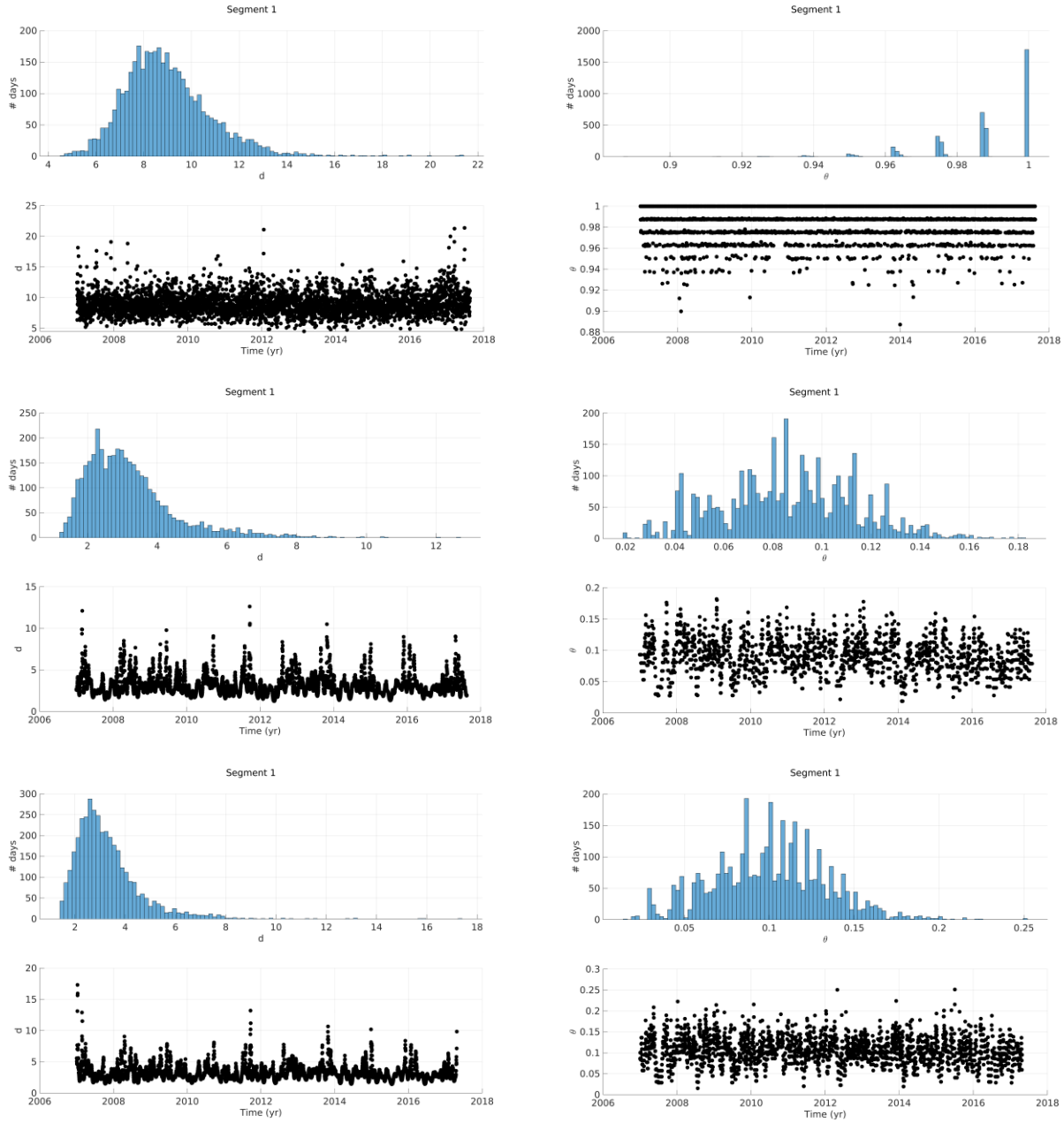

Fig. S26: Filter effects on the estimation of d (left column) and θ (right column) for segment #1. Top row: non-filtered case. Middle row: non-causally filtered case. Bottom row: causally filtered case.

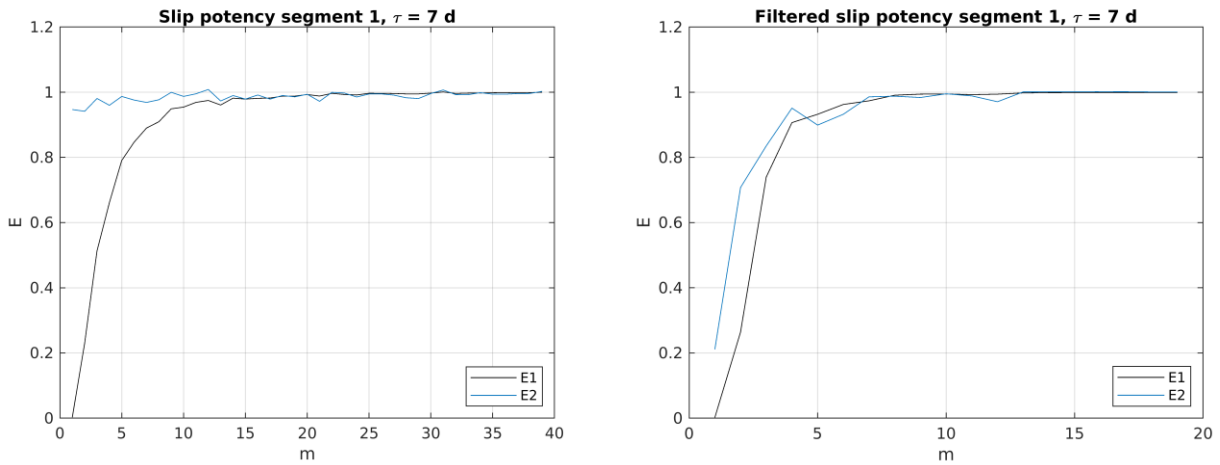

Fig. S27: Filter effects on the estimation of E_2 for segment #1. Left: Case for non-filtered time series. Right: Case for causally filtered time series.

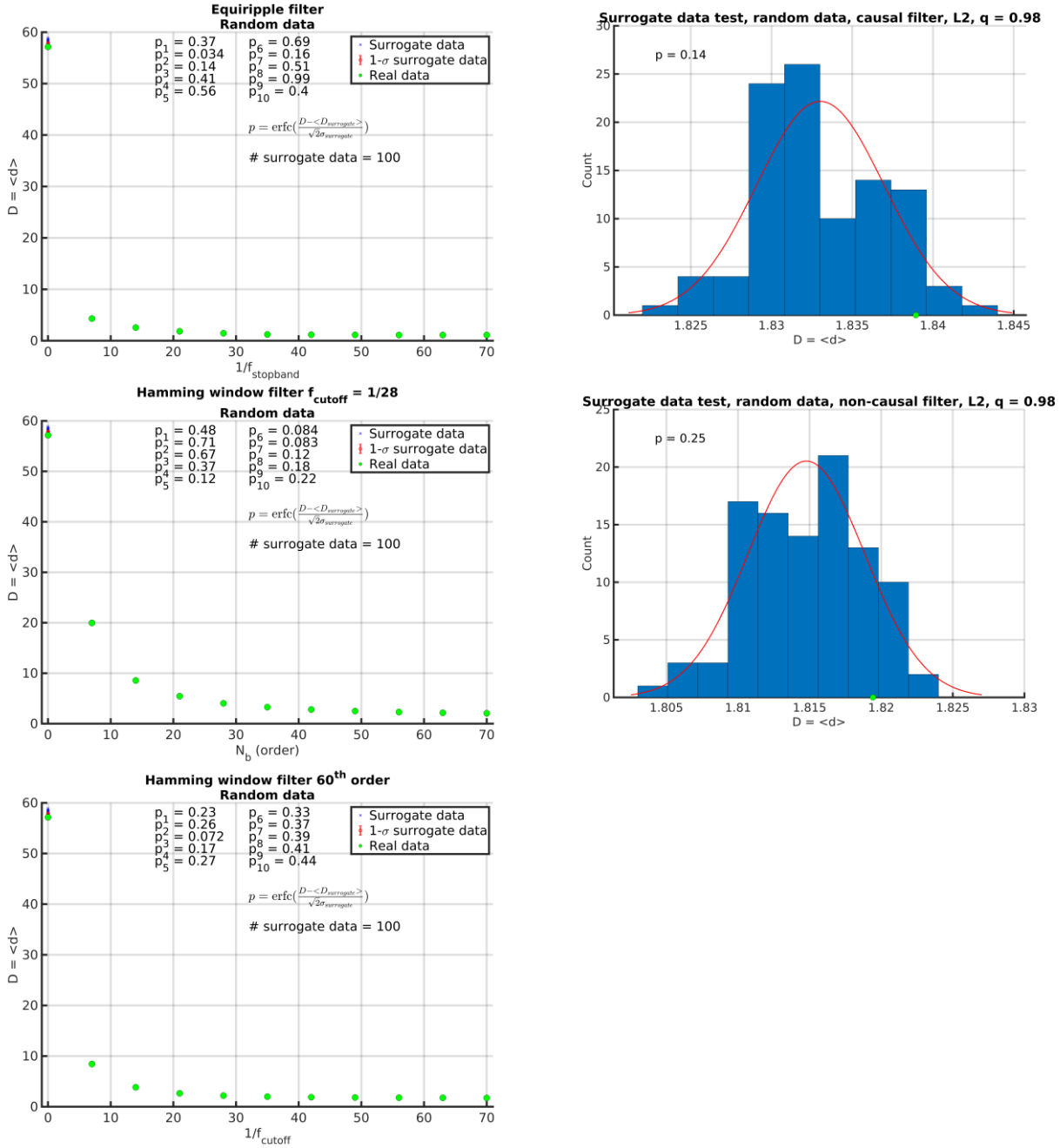

Fig. S28: Filter effects on random data. Left: Surrogate data test as in Fig. S22, but for (pseudo-)random data. The test is performed to verify the effects of the filters on stochastic time series. The high *p*-values reflect the fact that the blue crosses (i.e., the values of D as calculated on filtered surrogate data) are hidden below the green dots (i.e., the value of D calculated on the actual filtered data), indicating that we are not able to reject the null hypothesis for which the data can be described via a linear stochastic model. Right (top): Histogram showing the particular case of $\mathrm{EF}_{1/35}^{1/21}$, corresponding to the $p_3 = 0.14$ value in the top left panel (i.e., for $1/f_{stopband} = 21$). The green dot is the average dimension from the original random time series after causally filtering it. The red line shows the approximating Gaussian used to calculate the *p*-value. We use an L2 norm and a threshold quantile q = 0.98. Right (bottom): same as top right

panel, but for non-causally filtered time series. These results support our conclusion that the applied filters unlikely introduce an apparent chaotic dynamics to the slip potency rate time series of Cascadia.

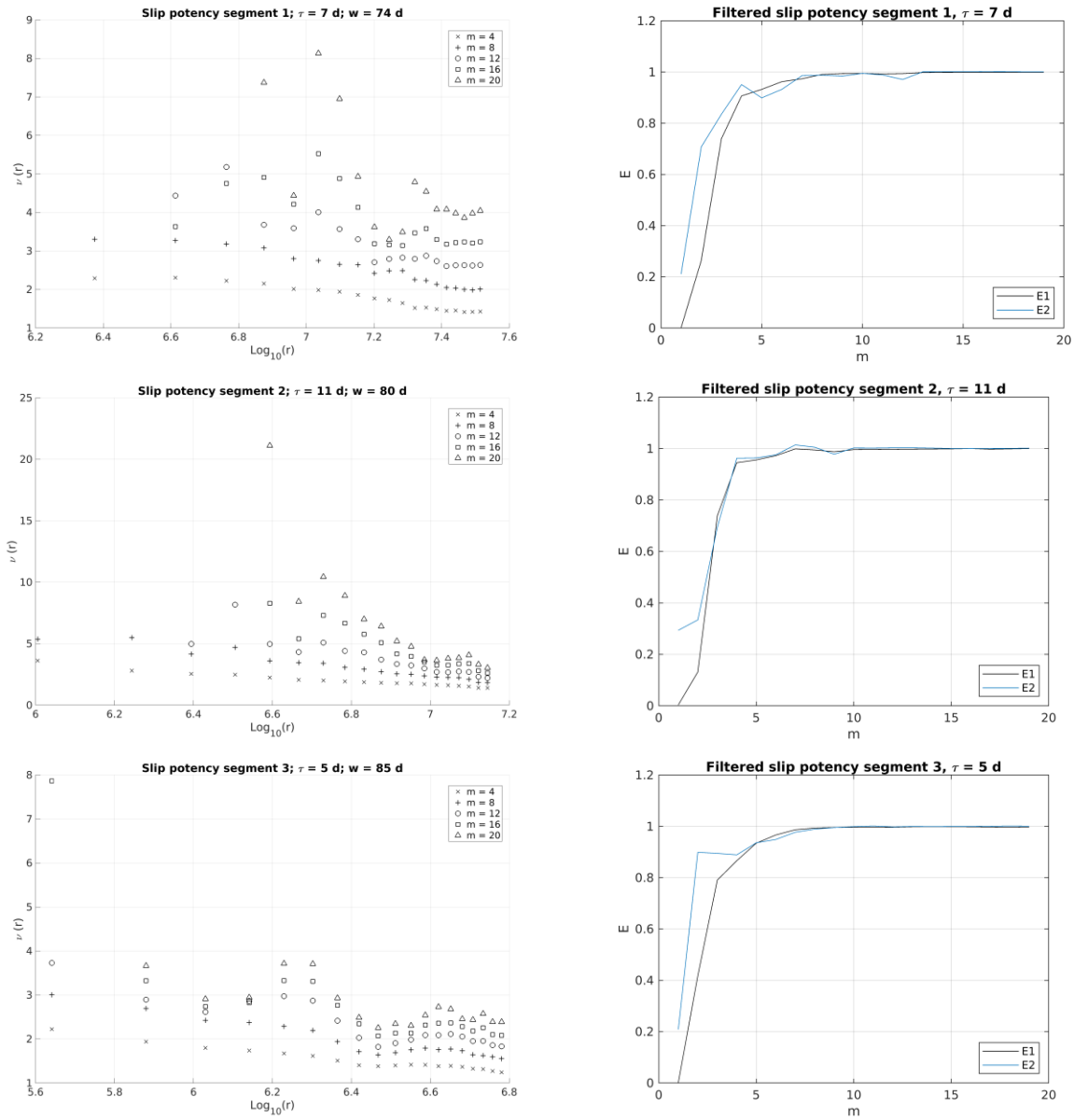

Fig. S29: Same as Fig. S8, but for slip potency instead of slip potency rate.

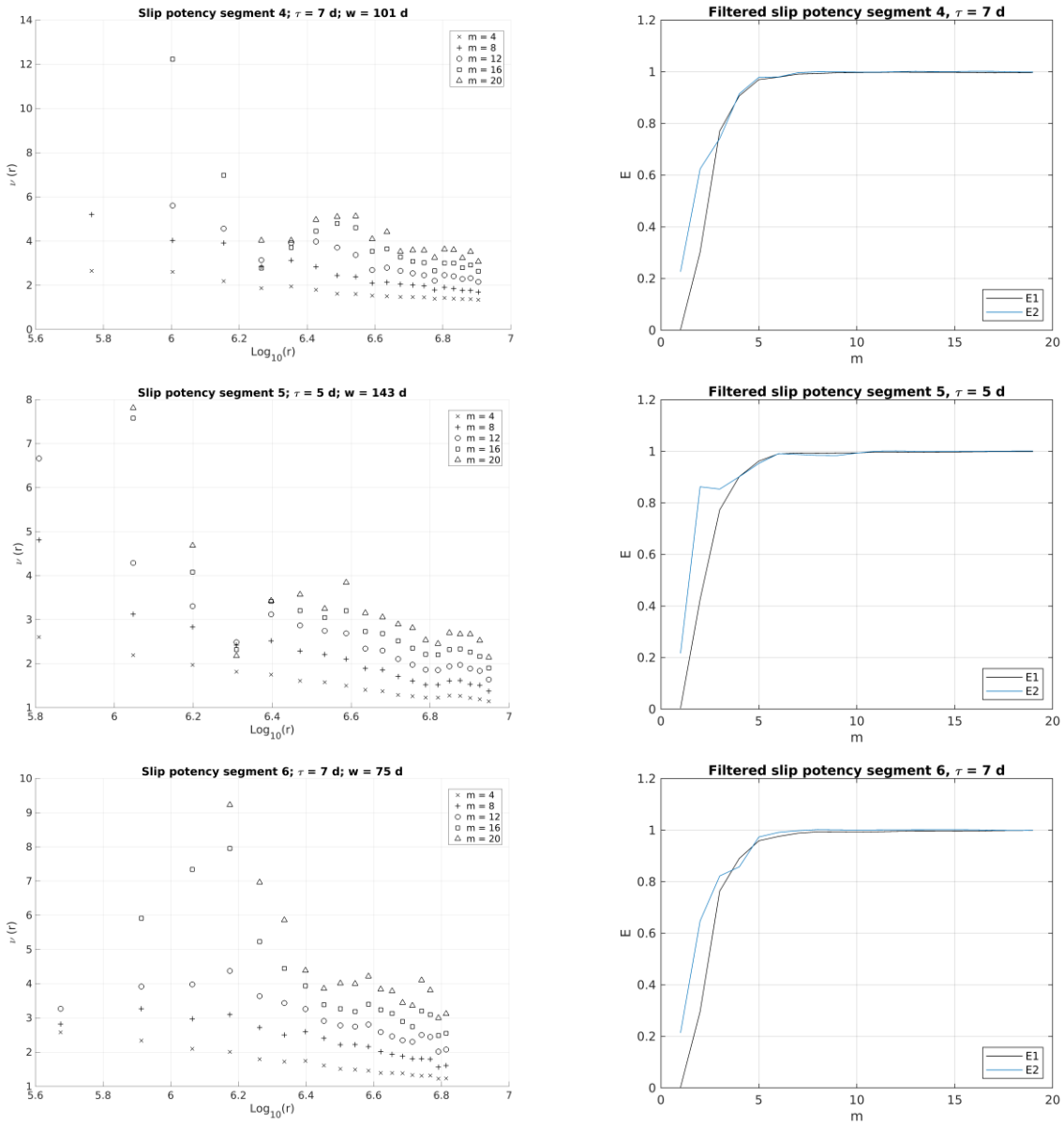

Fig. S30: Same as Fig. S29, but for segments #4, #5, and #6.

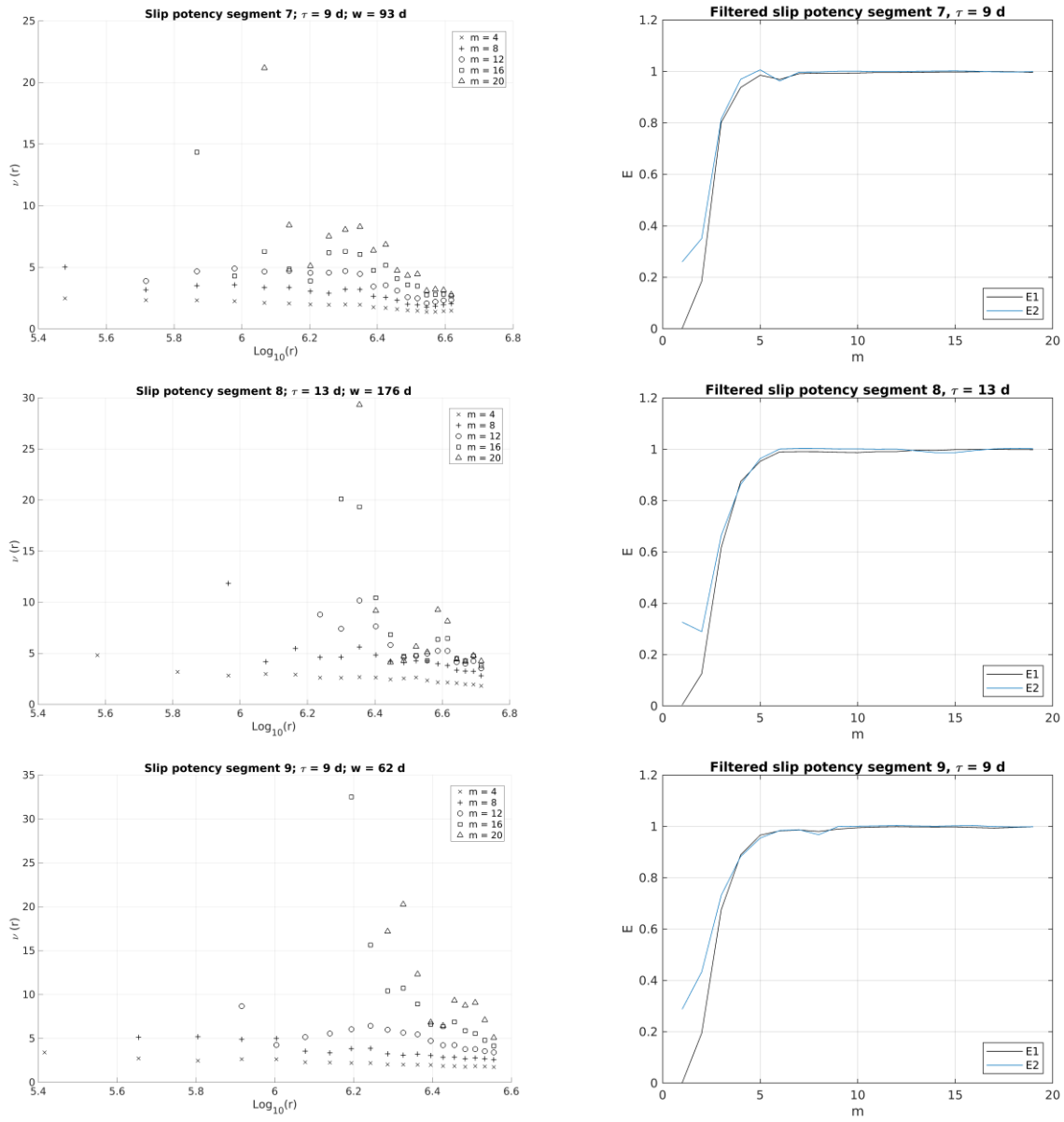

Fig. S31: Same as Fig. S29, but for segments #7, #8, and #9.

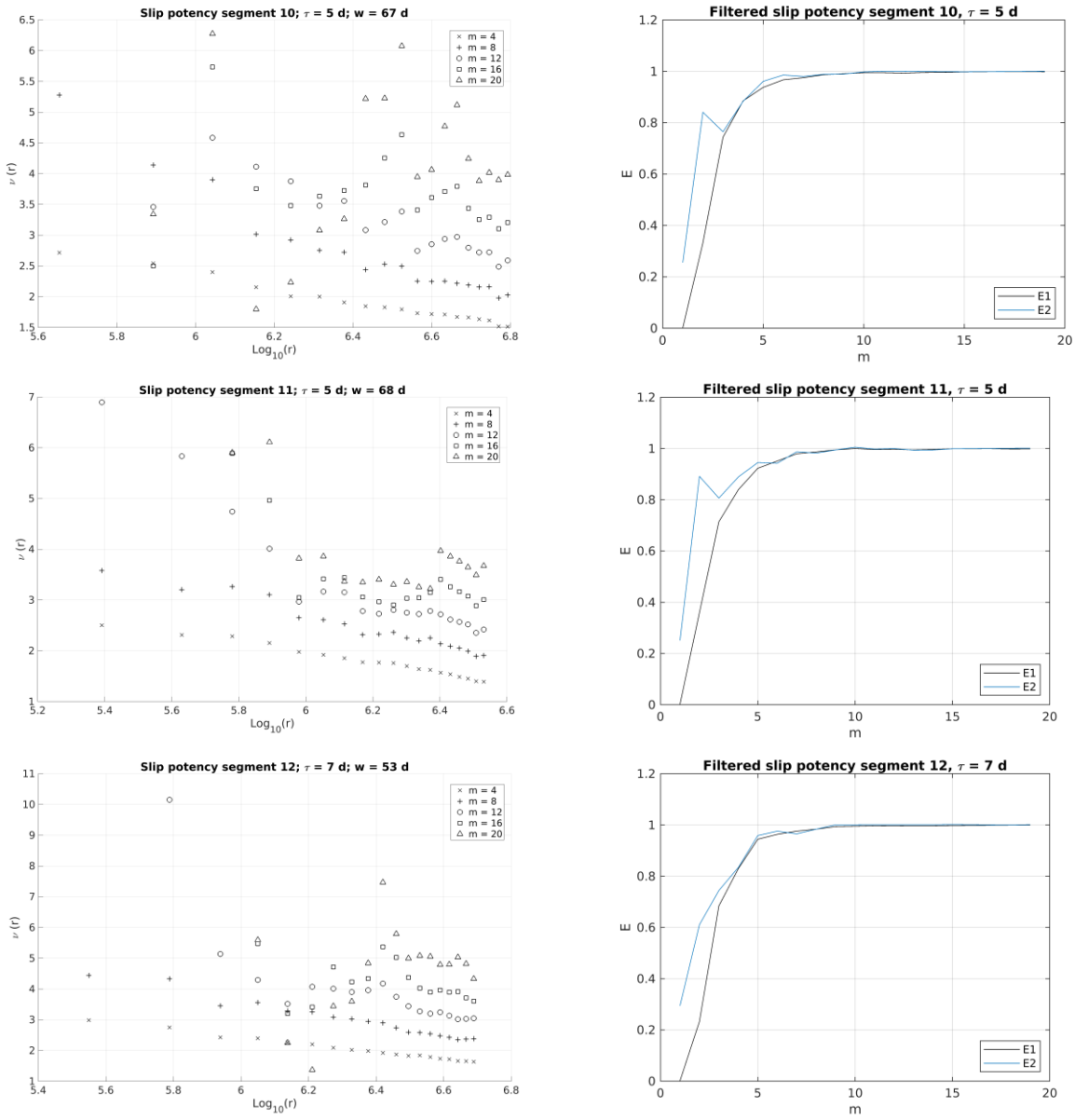

Fig. S32: Same as Fig. S29, but for segments #10, #11, and #12.

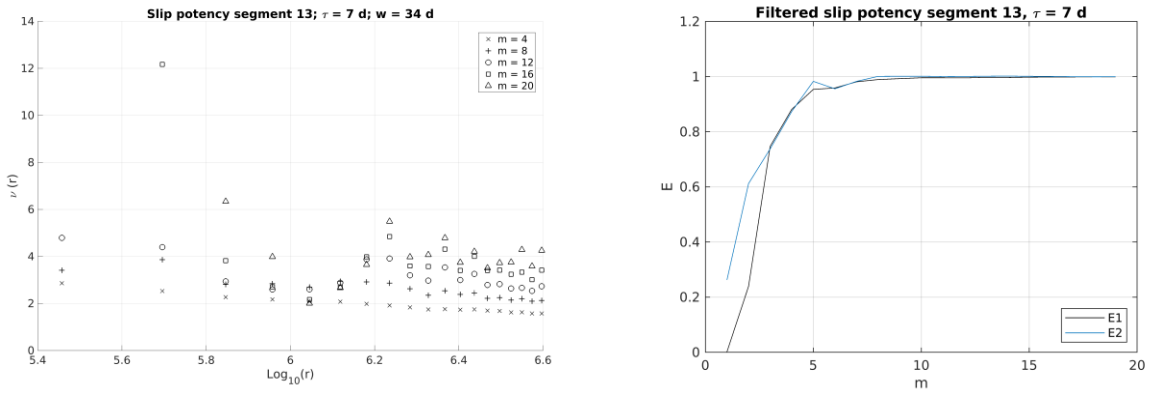

Fig. S33: Same as Fig. S29, but for segment #13.

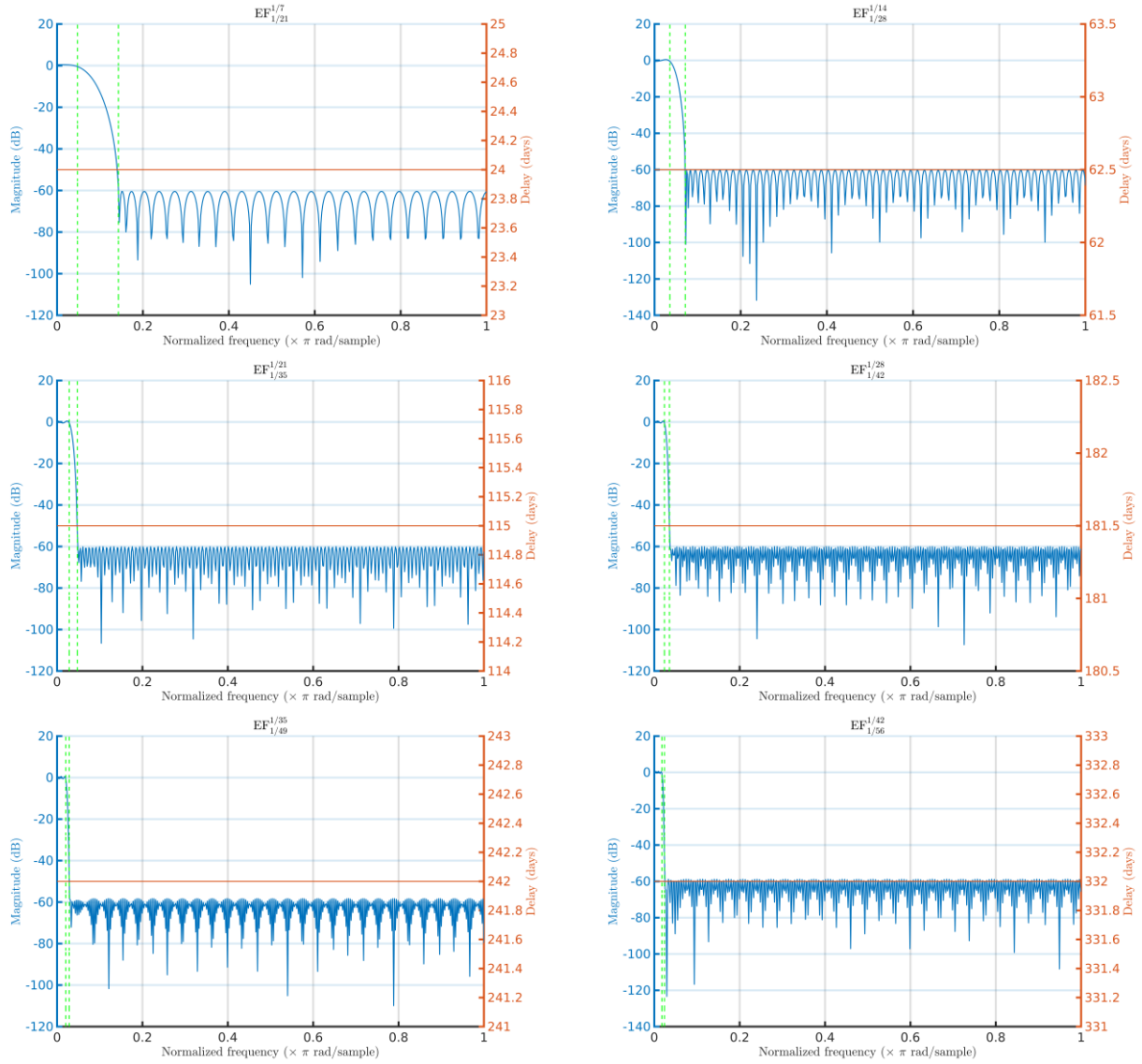

Fig. S34: Gain (blue) and group delay (orange) for the various combinations of the equiripple filter (EF). The green dashed lines indicate the normalized passband and stopband frequencies.

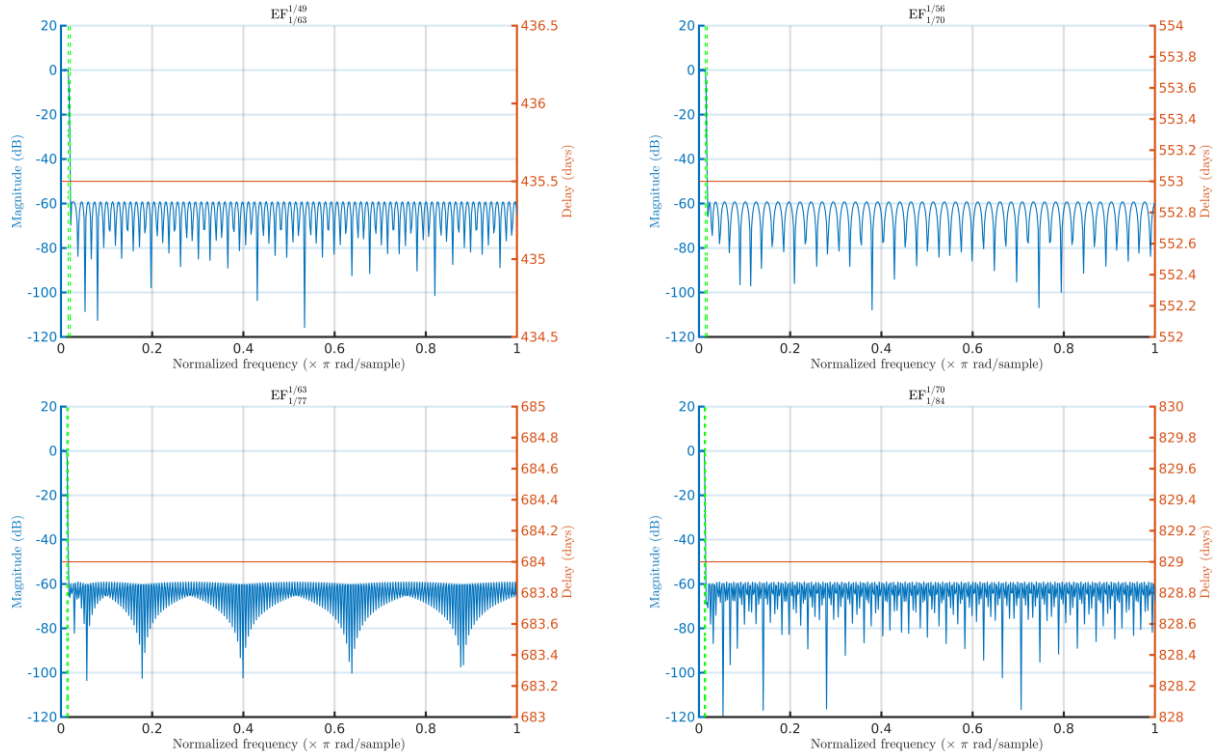

Fig. S35: Continuation of Fig. S34.

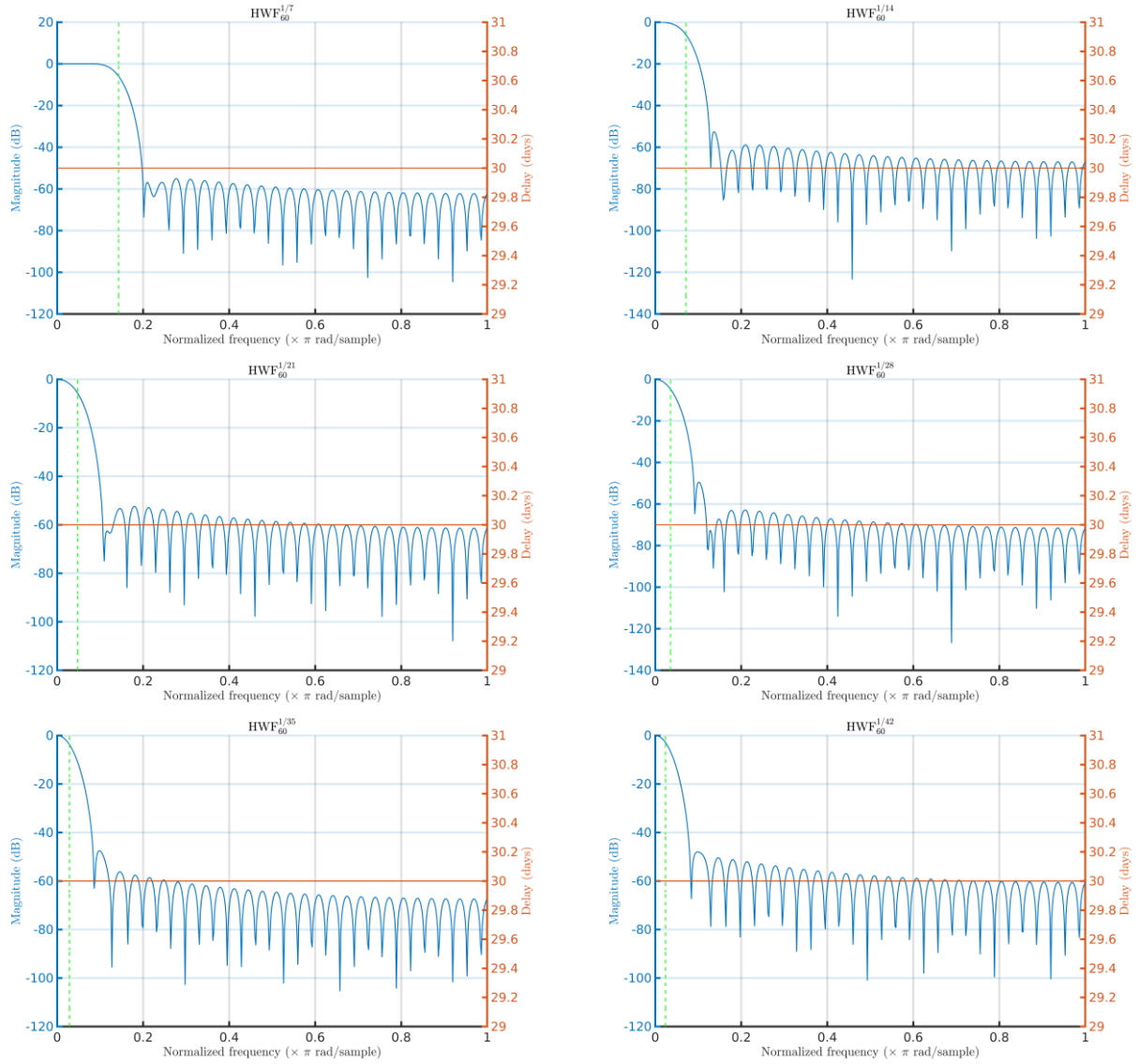

Fig. S36: As Fig. S34, but for a Hamming window filter (HWF) with constant $N_b = 60$ and variable f_{cutoff}.

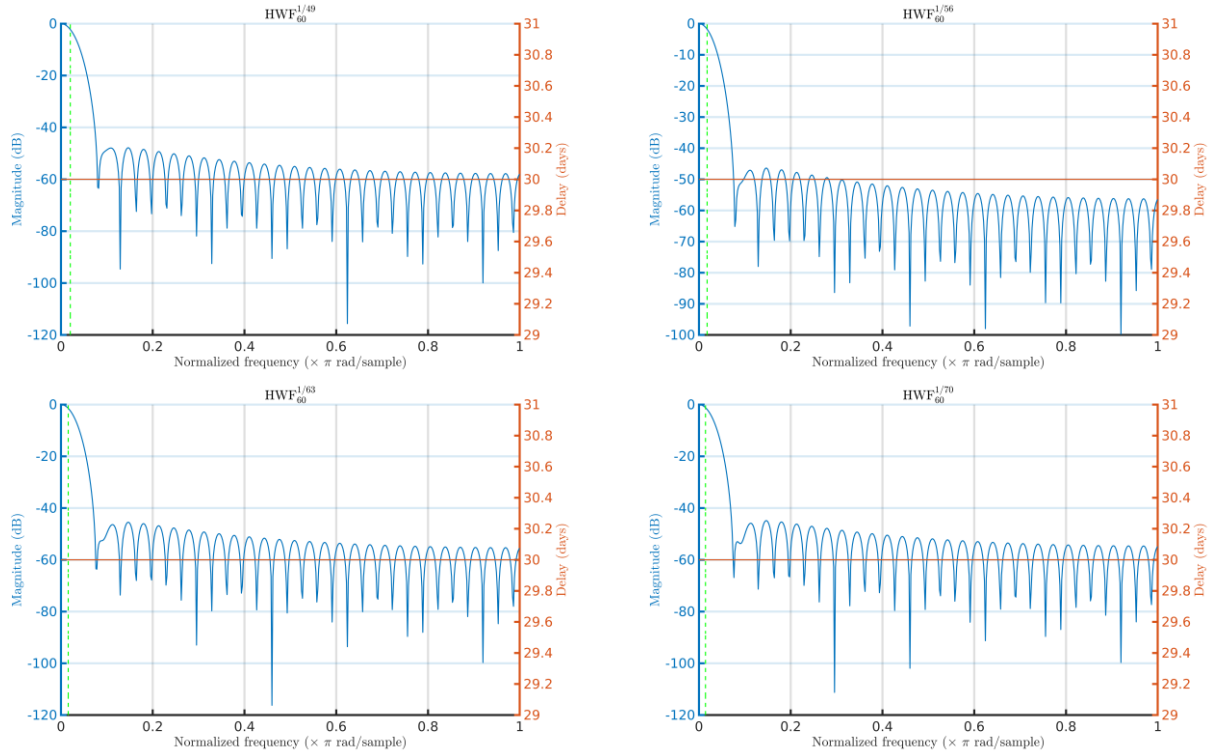

Fig. S37: Continuation of Fig. S36.

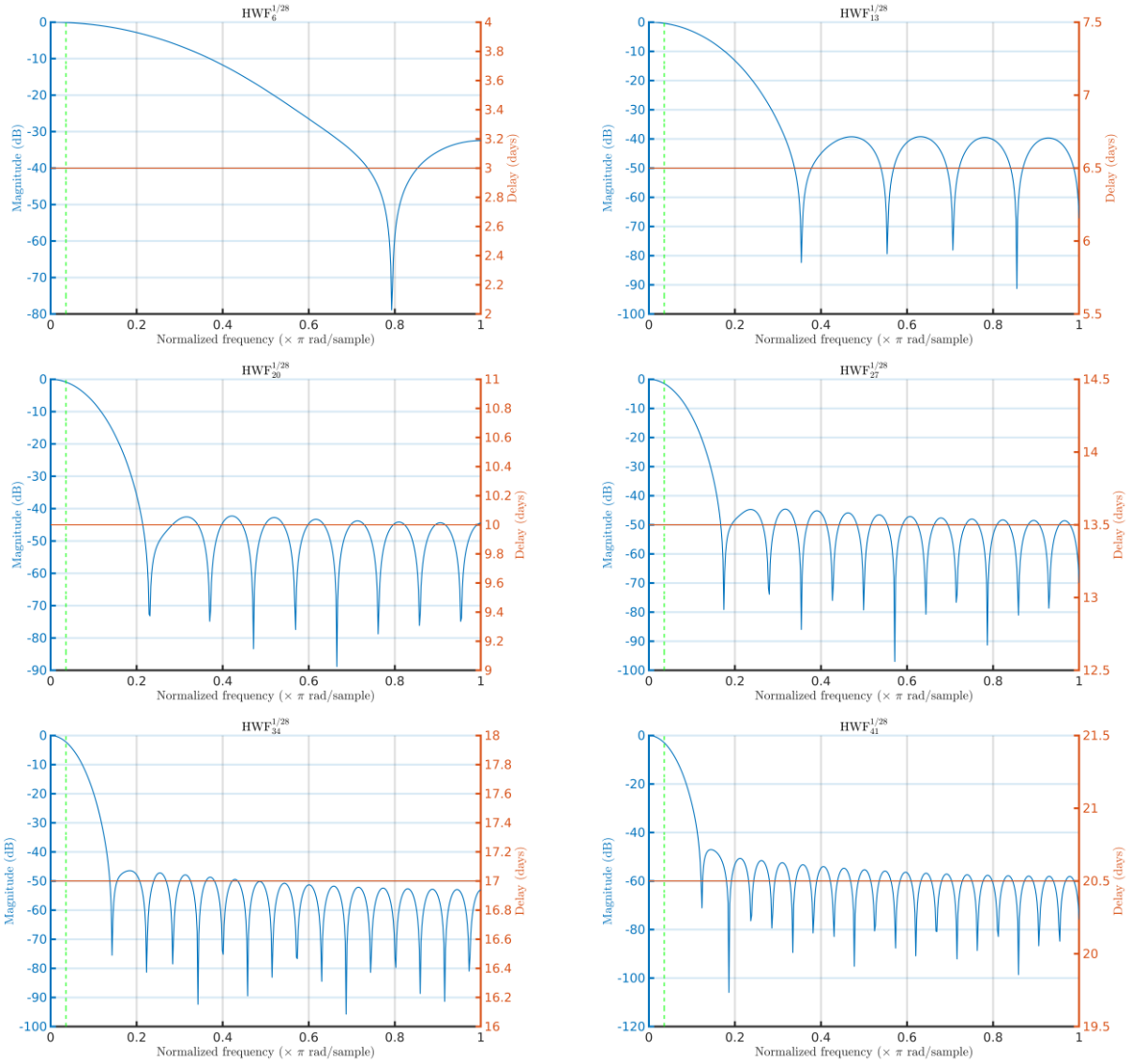

Fig. S38: As Fig. S34, but for a Hamming window filter (HWF) with constant $f_{cutoff} = 1/28$ and variable N_b.

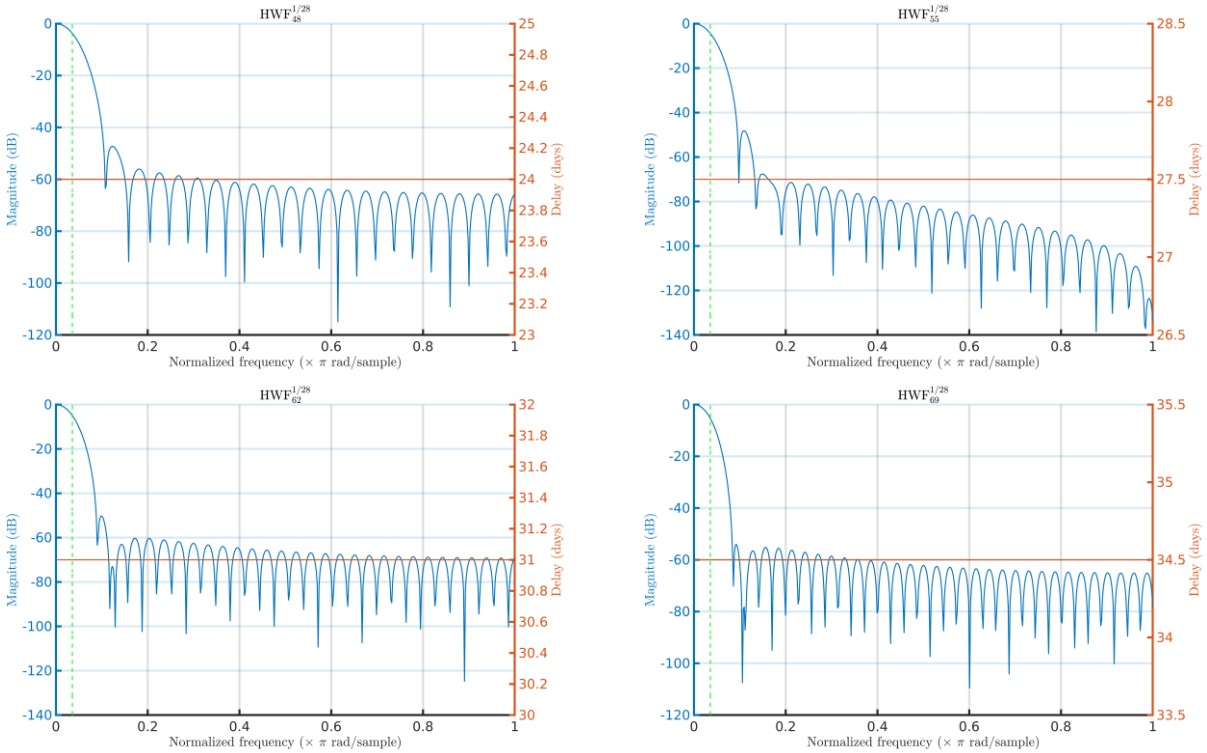

Fig. S39: Continuation of Fig. S38.

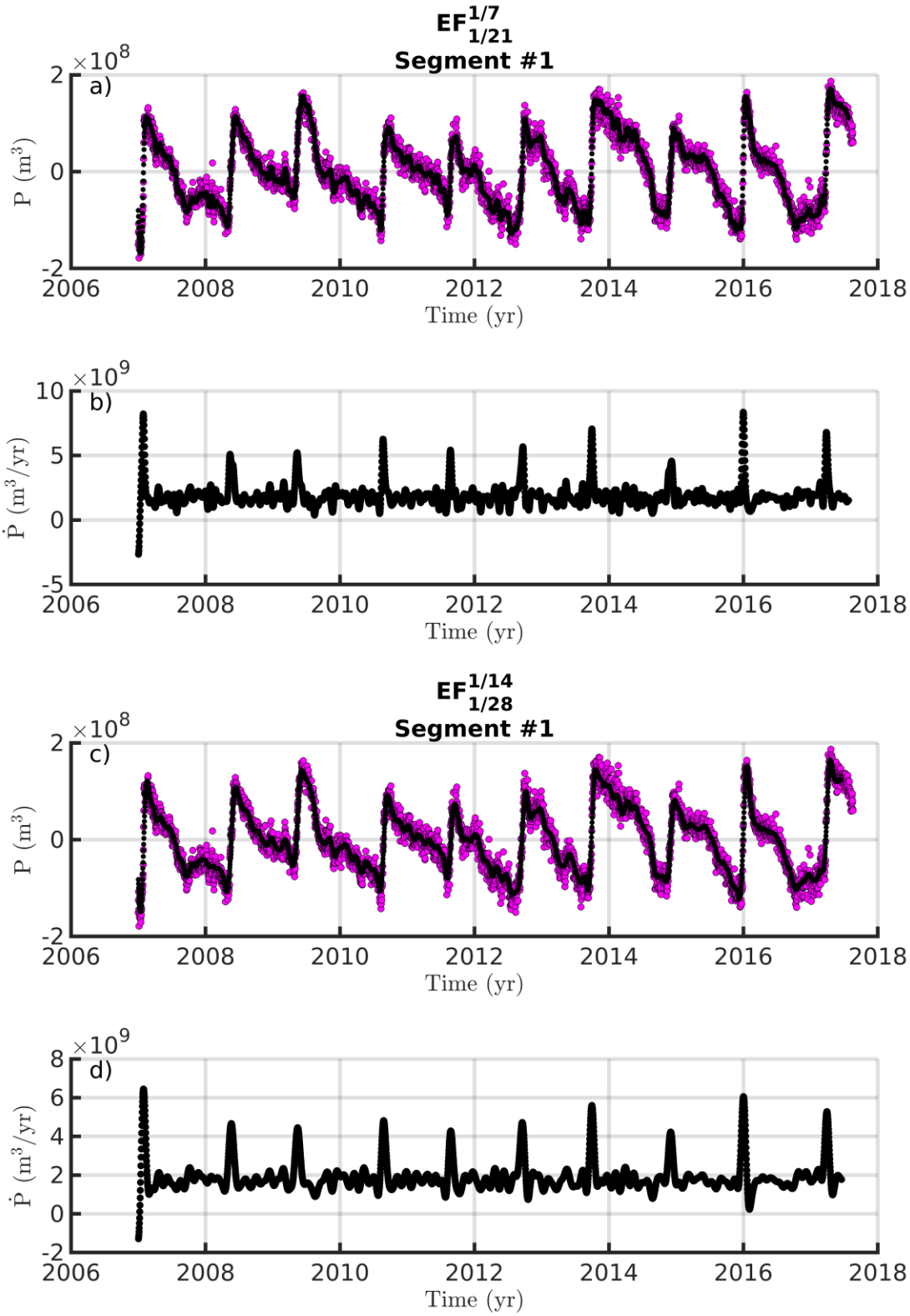

Fig. S40: Slip potency and slip potency rate temporal evolution for segment #1 and equiripple

filter (EF) with normalized passband and stopband frequencies specified by the sub- and super-script in the panels' title, respectively.

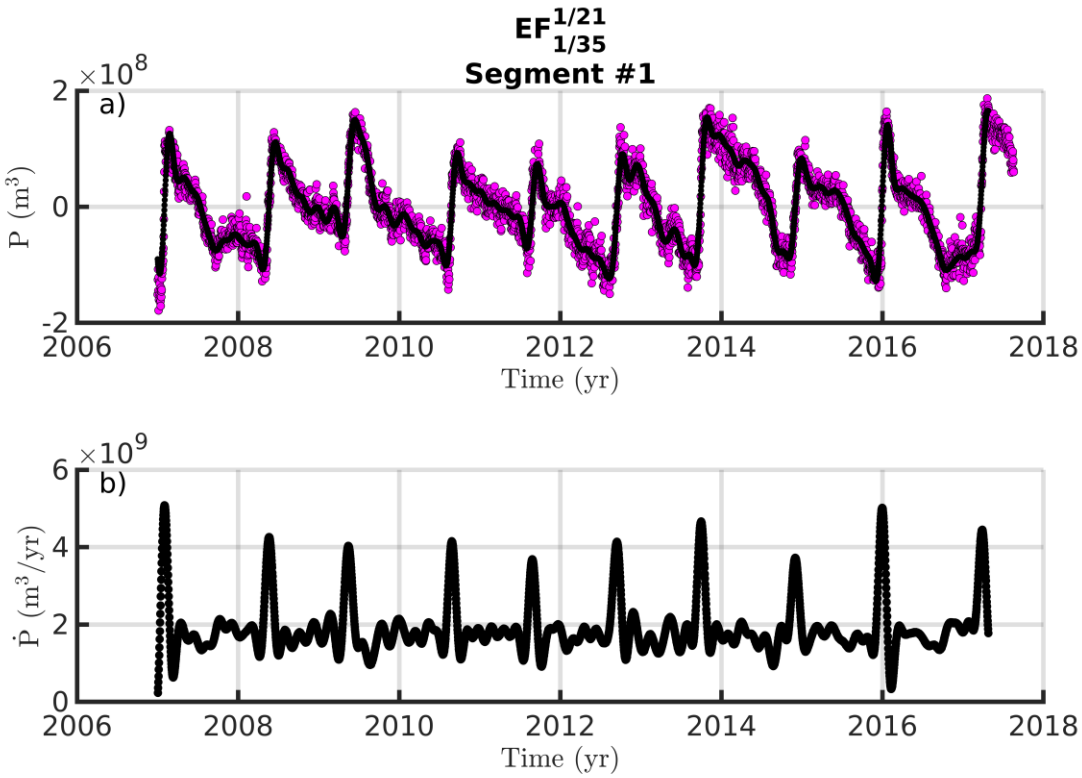

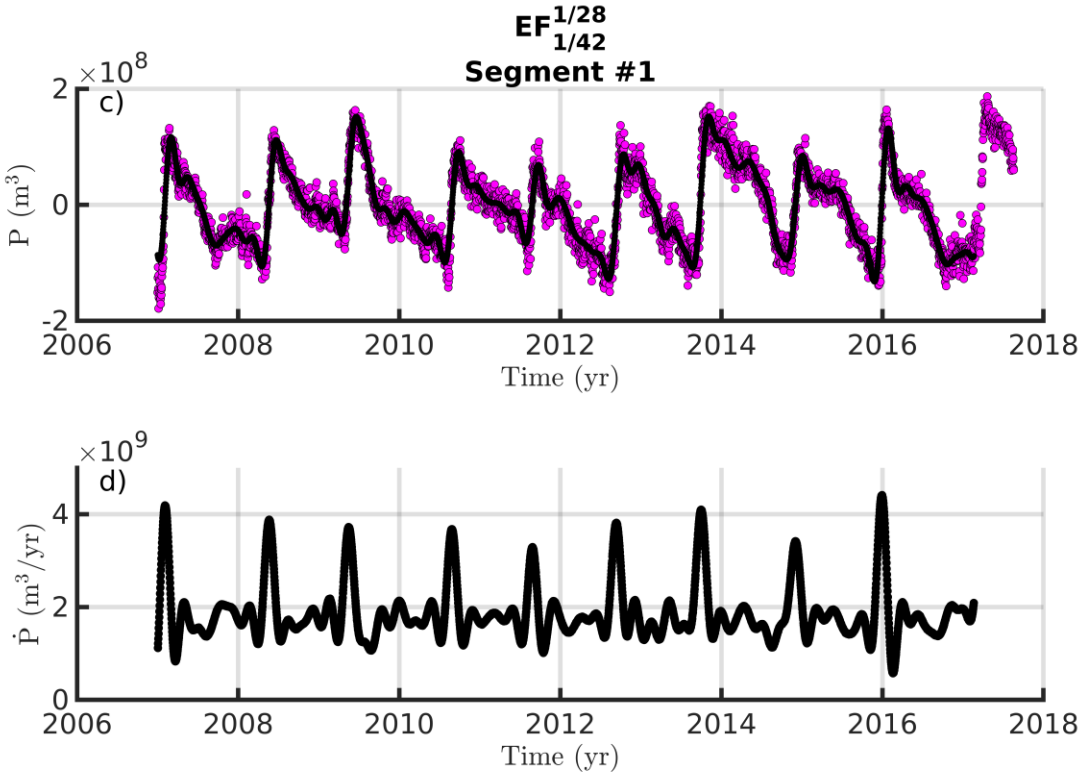

Fig. S41: Continuation of Fig. S40.

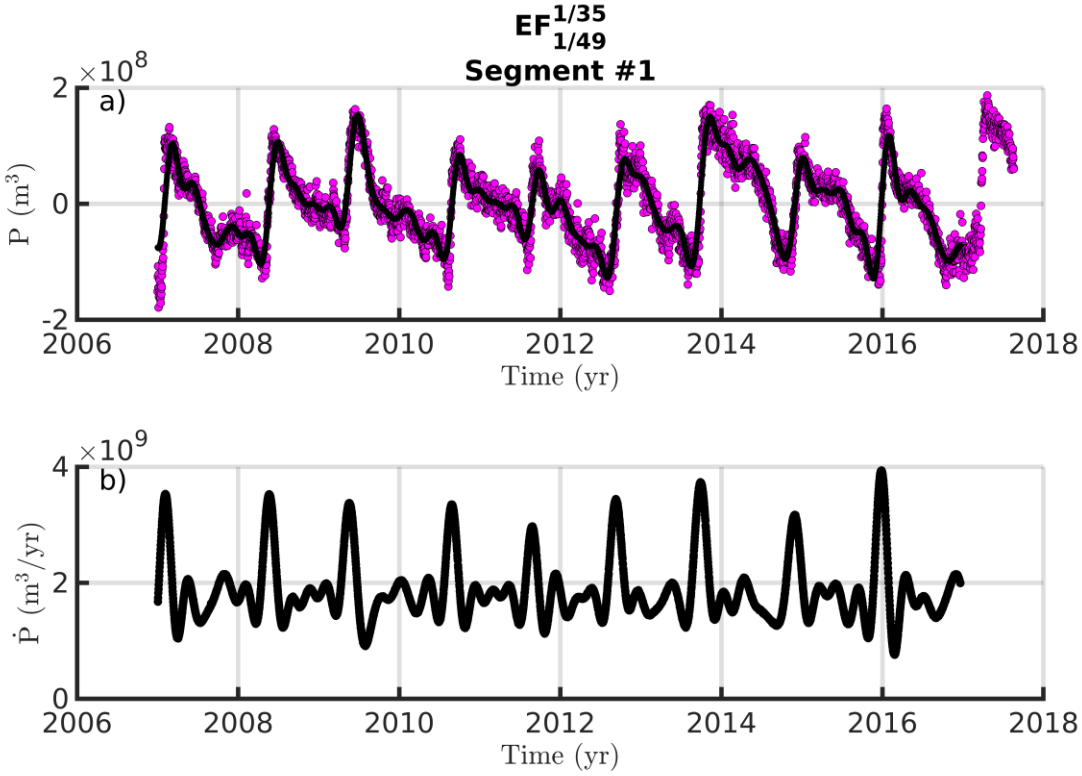

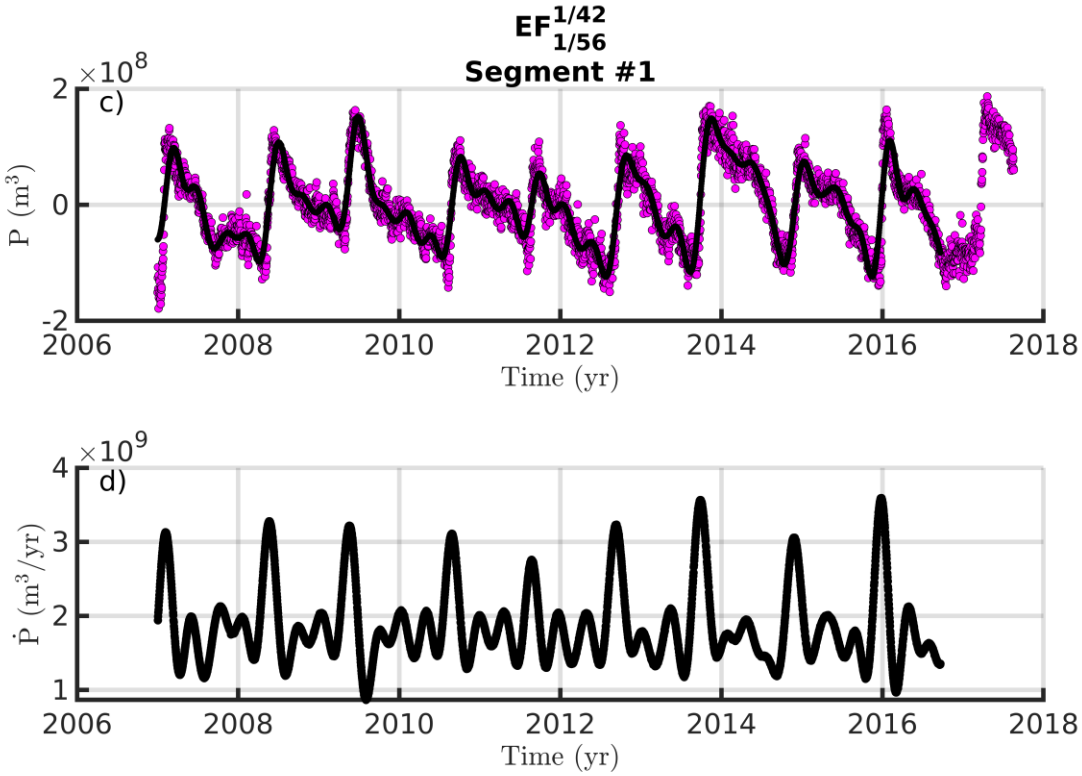

Fig. S42: Continuation of Fig. S40.

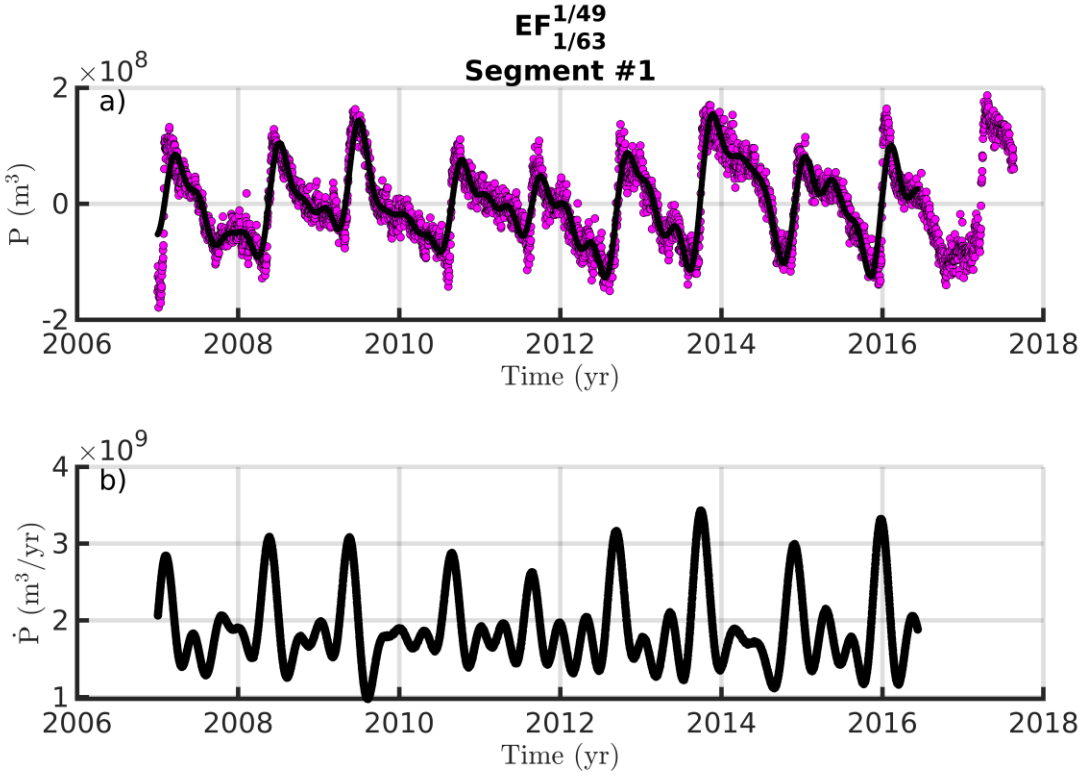

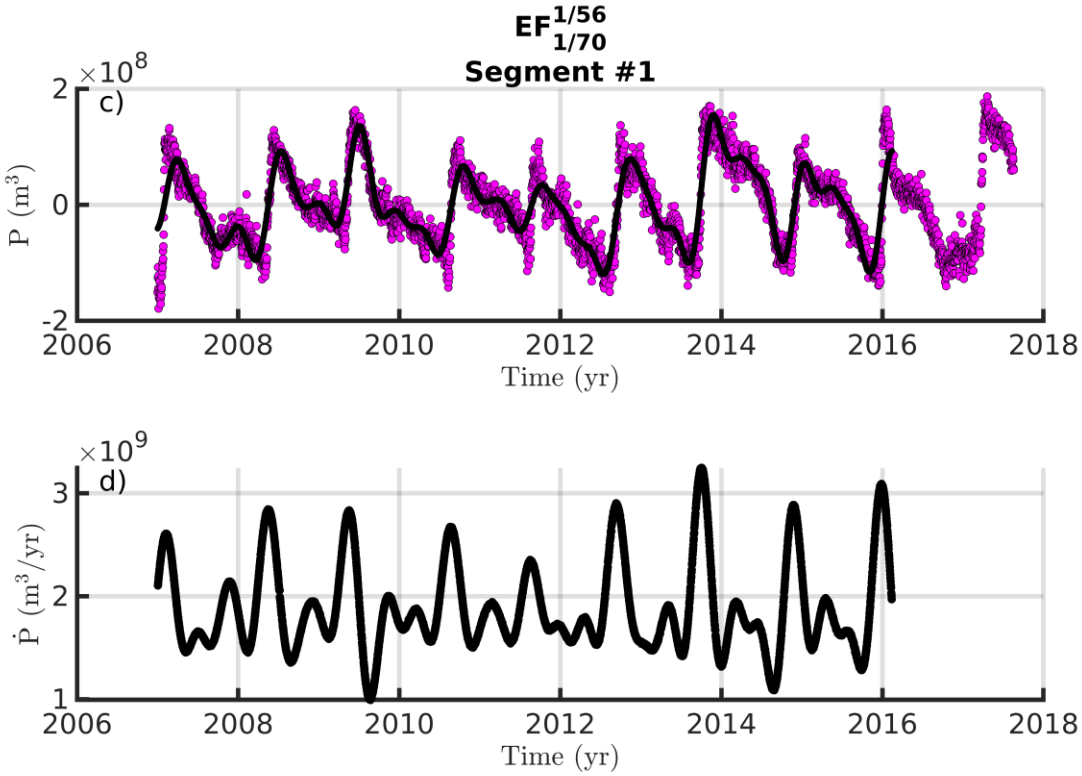

Fig. S43: Continuation of Fig. S40.

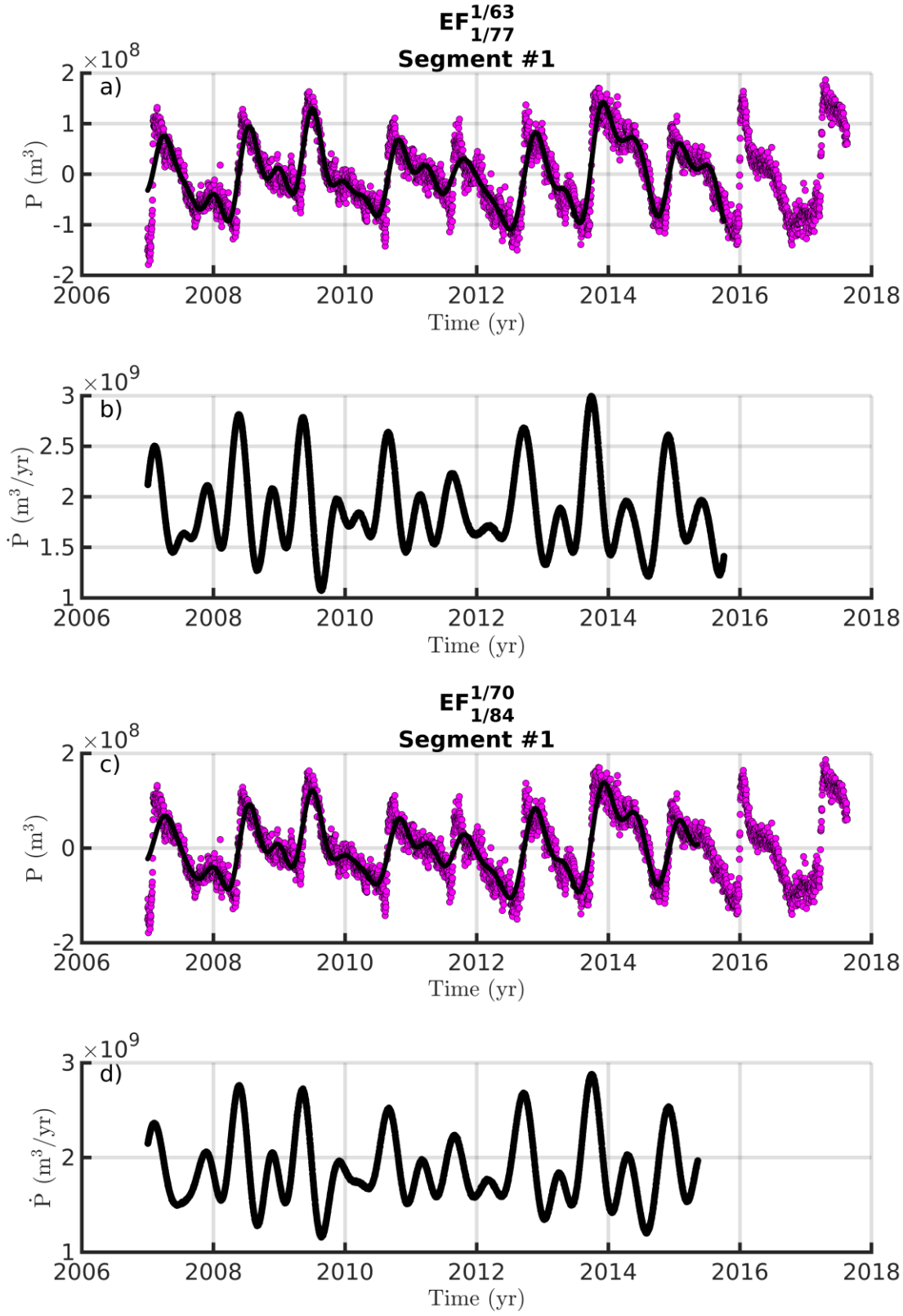

Fig. S44: Continuation of Fig. S40.

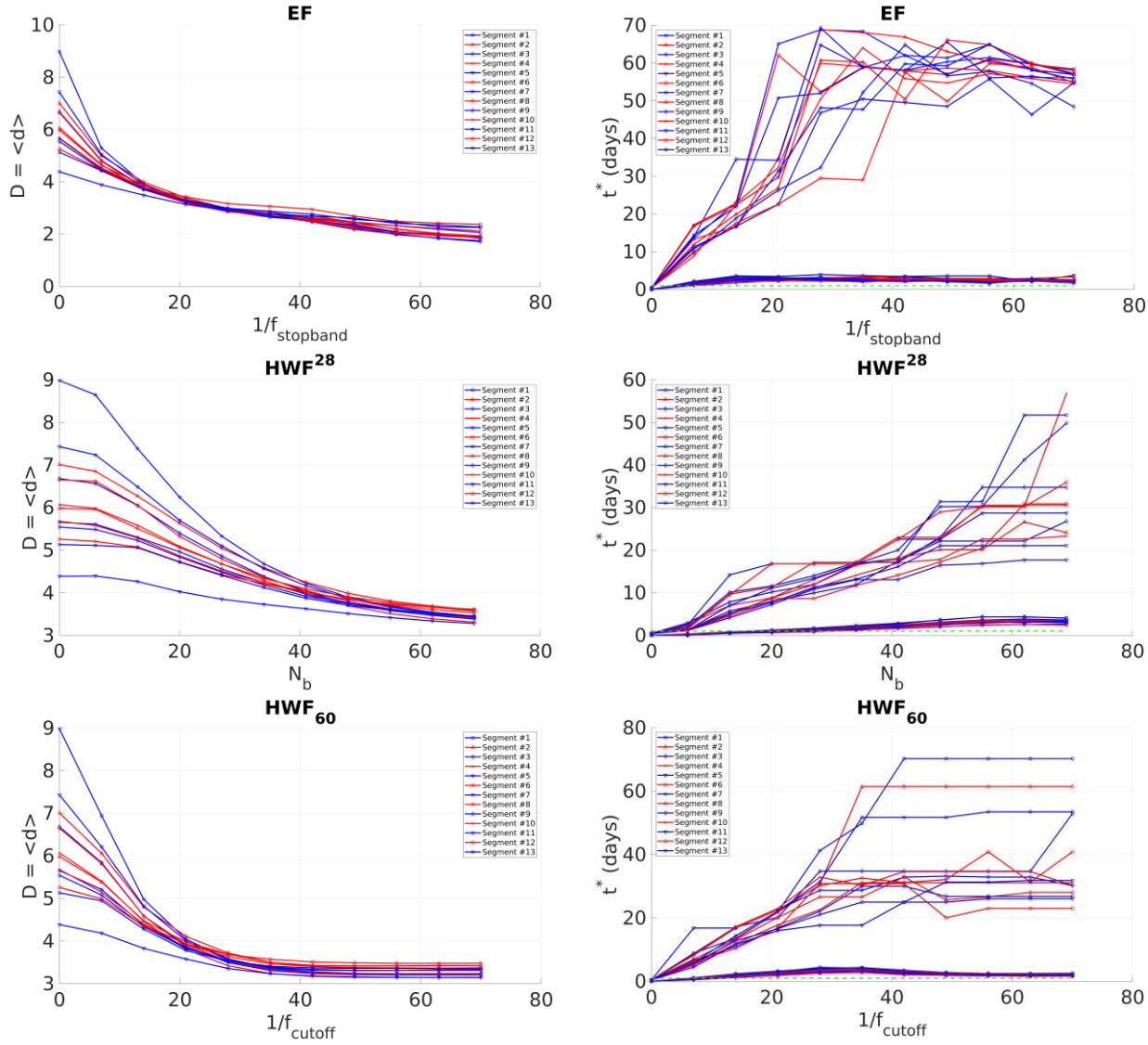

Fig. S45: Variability of D, t^*_{min} and t^*_{max} estimated via EVT as a function of filters and filter parameters.